LEVEL II

CM-CCM-79-3

October 1979

Interception of Hostile Communications

By Don J. Torrieri

U.S. Army Materiel Development
and Readiness Command
**Countermeasures/
Counter-countermeasures Office**
2800 Powder Mill Road
Adelphi, MD 20783

The findings in this report are not to be construed as an official Department of the Army position unless so designated by other authorized documents.

Citation of manufacturers' or trade names does not constitute an official indorsement or approval of the use thereof.

Destroy this report when it is no longer needed. Do not return it to the originator.

Editorial review and camera-ready copy by Technical Reports Branch, Harry Diamond Laboratories

UNCLASSIFIED

SECURITY CLASSIFICATION OF THIS PAGE (When Data Entered)

REPORT DOCUMENTATION PAGE

READ INSTRUCTIONS BEFORE COMPLETING FORM

1. REPORT NUMBER: CM-CCM-79-3	2. GOVT ACCESSION NO.
3. RECIPIENT'S CATALOG NUMBER	
4. TITLE (and Subtitle): Interception of Hostile Communications	5. TYPE OF REPORT & PERIOD COVERED: Technical Report
6. PERFORMING ORG. REPORT NUMBER	
7. AUTHOR(s): Don J. Torrieri	8. CONTRACT OR GRANT NUMBER(s)
9. PERFORMING ORGANIZATION NAME AND ADDRESS: Countermeasures/Counter-countermeasures Office, 2800 Powder Mill Road, Adelphi, MD 20783	10. PROGRAM ELEMENT, PROJECT, TASK AREA & WORK UNIT NUMBERS: Program Ele: 6.37.49.A, DA: 1S463749D462
11. CONTROLLING OFFICE NAME AND ADDRESS: U.S. Army Materiel Development & Readiness Command, Alexandria, VA 22333	12. REPORT DATE: October 1979
	13. NUMBER OF PAGES: 70
14. MONITORING AGENCY NAME & ADDRESS (if different from Controlling Office)	15. SECURITY CLASS. (of this report): Unclassified
	15a. DECLASSIFICATION/DOWNGRADING SCHEDULE

16. DISTRIBUTION STATEMENT (of this Report)

Approved for public release; distribution unlimited.

17. DISTRIBUTION STATEMENT (of the abstract entered in Block 20, if different from Report)

18. SUPPLEMENTARY NOTES

ERADCOM Project: T499TA
DRCMS Code: 643749.4620011

19. KEY WORDS (Continue on reverse side if necessary and identify by block number)

Interception	Microscan receiver
Radiometer	Frequency estimation
Direction finding	Countermeasures
Detection	Interferometer
Cross correlation	

20. ABSTRACT (Continue on reverse side if necessary and identify by block number)

Whatever the ultimate purpose of an interception system is, it nearly always must achieve the three basic functions of detection, frequency estimation, and direction finding. The fundamental concepts and issues of these three elements of interception are presented at the systems level, assuming that little is known about the signals to be intercepted. The capabilities of radiometers and cross correlators for detection are determined. Channelized,

DD FORM 1 JAN 73 1473 EDITION OF 1 NOV 65 IS OBSOLETE

UNCLASSIFIED

SECURITY CLASSIFICATION OF THIS PAGE (When Data Entered)

410947

Item 20 Cont'd.

discrete Fourier transform, acousto-optical, instantaneous frequency measurement, scanning superheterodyne, and microscan receivers for frequency estimation are described and analyzed. Direction finding by energy comparison systems with radiometers is analyzed. The two types of interferometers are discussed.

CONTENTS

		Page
1.	INTRODUCTION	5
2.	DETECTION	5
	2.1 Radiometer	8
	2.2 Channelized Radiometer	15
	2.3 Cross Correlator	19
3.	FREQUENCY ESTIMATION	26
	3.1 Channelized Receiver	26
	3.2 Spectrum Analysis with Discrete Fourier Transform	28
	3.3 Acousto-optical Receiver	31
	3.4 Instantaneous Frequency Measurement	33
	3.5 Scanning Superheterodyne Receiver	35
	3.6 Microscan Receiver	41
4.	DIRECTION FINDING	47
	4.1 Energy Comparison Systems	47
	4.2 Interferometer	56
5.	*CONCLUSIONS*	60
	LITERATURE CITED	63
	GLOSSARY OF PRINCIPAL SYMBOLS	65
	DISTRIBUTION	69

FIGURES

1	Correlation detector	6
2	Optimum detector for pulsed sinusoid of unknown frequency	7
3	Radiometer	8
4	Channelized radiometers	15
5	Cross correlator	20
6	Channelized receiver with filters arranged in successive stages	28
7	Acousto-optical spectrum analyzer	32

Figures (Cont'd)

		Page
8	Acousto-optical diffraction geometry for input at single frequency	32
9	Array of Bragg cells for simultaneous frequency estimation and direction finding	34
10	Instantaneous frequency measurement receiver	34
11	Scanning superheterodyne receiver	36
12	Time-frequency diagram for scanning superheterodyne receiver	37
13	Microscan receivers	41
14	Response of scanning superheterodyne and microscan receivers to simultaneous signals	44
15	Stationary multibeam system	48
16	Adjacent antenna radiation patterns	48
17	Root-mean-square error versus arrival angle for different beam widths	52
18	Root-mean-square error versus arrival angle for optimal beam widths and different values of γ	52
19	Rotating beam system	53
20	Rotating monopulse system	54
21	Interferometers	57

1. INTRODUCTION

Interception of hostile communications is attempted for many diverse reasons, such as reconnaissance, surveillance, position fixing, identification, or a prelude to jamming. Different purposes require different systems, but whatever the purpose, an interception system nearly always must achieve the three basic functions of detection, frequency estimation, and direction finding. Although these three elements of interception are usually integrated in a practical system, they are discussed separately in this paper for clarity of presentation. The basic concepts and issues of the three elements are presented at the systems level, assuming that little is known about the signals to be intercepted. Primarily because of the rapidly changing technological base, the implementation and the engineering details of the interception systems are not addressed. Although this paper is concerned with the interception of communications, only slight modifications of the results are required to apply them to the interception of radar.

The potential interceptor has at least one major advantage over the communicators. The accuracies of detection, frequency estimation, and direction finding are determined by the energy of the entire message transmitted, which may include many symbols. In contrast, the intended receiver makes decisions with accuracies determined by the energy of each transmitted symbol. From another point of view, the intended receiver generally must make many separate decisions, whereas the interception receiver must make only a few decisions.

2. DETECTION

If the form and the parameters of the signal to be intercepted, $s(t)$, were known, optimum detection in white Gaussian noise, $n(t)$, could be accomplished by a matched filter or an ideal correlator. Figure 1 depicts a correlator for the received signal, $r(t) = s(t) + n(t)$, and an observation interval, T. The comparator input is compared with a fixed threshold level, V_T, to determine the presence of an intercepted signal. It is a standard result that the probability of false alarm, P_F, and the probability of detection, P_D, are given by[1]

$$P_F = \frac{1}{2} \operatorname{erfc} \left[\frac{V_T}{(N_0 E)^{1/2}} \right], \tag{1}$$

$$P_D = \frac{1}{2} \operatorname{erfc} \left[\frac{V_T}{(N_0 E)^{1/2}} - \left(\frac{E}{N_0} \right)^{1/2} \right], \tag{2}$$

[1] *A. Whalen, Detection of Signals in Noise, Academic Press, Inc., New York (1971).*

where E is the signal energy, $N_0/2$ is the noise power spectral density, and the complementary error function is defined as

$$\text{erfc}\ (x) = \frac{2}{\sqrt{\pi}} \int_x^\infty \exp\left(v^2\right) dv \ . \tag{3}$$

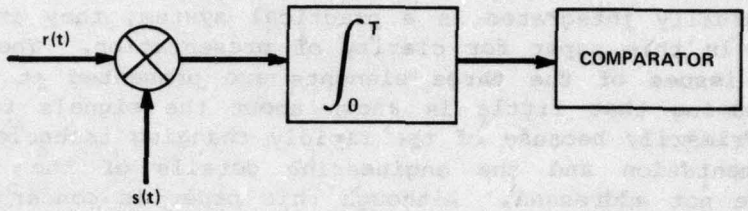

Figure 1. Correlation detector.

Denoting the inverse complementary error function by erfc^{-1}, we define

$$\beta = \text{erfc}^{-1}\left(2P_F\right) , \tag{4}$$

$$\xi = \text{erfc}^{-1}\left(2P_D\right) . \tag{5}$$

From equations (1) and (2), we can calculate the value of E/N_0 necessary to ensure specified P_F and P_D. The result is

$$\frac{E}{N_0} = (\beta - \xi)^2 . \tag{6}$$

Although the ideal correlator cannot be used when s(t) is unknown, equation (6) provides a basis of comparison for more realistic interception receivers.

To detect the presence of an unknown signal, we assume that the intercepted signal has random phase and frequency and an unknown constant amplitude. The signal frequency is assumed to be one of M possible values; that is, the band to be searched is divided into M channels with center frequencies ω_1, ω_2, etc. To each discrete frequency, ω_i, we assign a hypothesis, H_i. Thus, the multiple alternative hypotheses over an observation interval are

$$H_0: r(t) = n(t), \quad 0 \le t \le T ,$$

$$H_1: r(t) = A \sin\left(\omega_1 t + \theta_1\right) + n(t) , \quad 0 \le t \le T ,$$

$$\vdots$$

$$H_M: r(t) = A \sin\left(\omega_M t + \theta_M\right) + n(t) , \quad 0 \le t \le T ,$$

where the θ_i are phase angles. We assume that the phase angles are uniformly distributed and that each frequency is equally likely to occur. A comparison of the likelihood ratios[1] yields the receiver depicted in figure 2. The decision rule is the following: choose H_i, $i = 1, \ldots, M$, if the largest envelope detector output is greater than the threshold, and choose H_0 otherwise. If a signal is detected, this receiver automatically identifies the frequency as the center frequency of the filter with the largest output.

The matched filters of figure 2 are matched to intercepted signals that are pulsed sinusoids. To accommodate more general, unknown signals, the matched filters could be replaced by bandpass filters. However, such a replacement would give a detector that is not necessarily optimum.

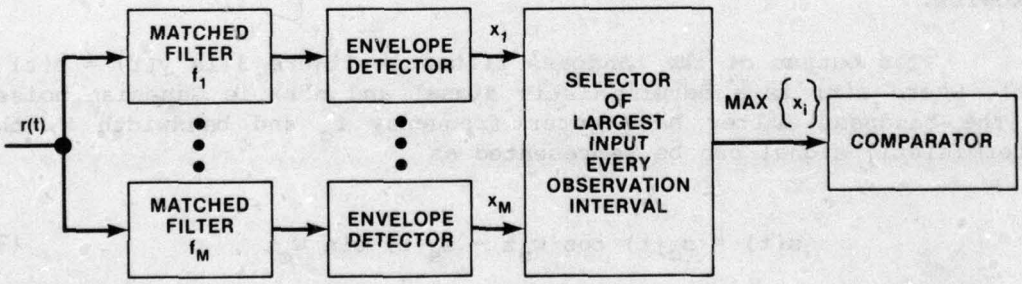

Figure 2. Optimum detector for pulsed sinusoid of unknown frequency.

[1] *A. Whalen, Detection of Signals in Noise, Academic Press, Inc., New York (1971).*

There remain other problems with this receiver. It is doubtful that the envelope detectors can function efficiently against some signal forms. Furthermore, the receiver is designed to operate on a single pulse. Multiple-pulse operation, which may be necessary for detection at low signal power levels, requires additional hardware.

2.1 Radiometer

Another approach is to model the signal as a stationary Gaussian process with a flat power spectral density. Assuming that the noise present is white and Gaussian, detection theory yields the optimum receiver depicted in figure 3, which is called an energy detector or a radiometer.[2] This receiver has the major advantages that it requires relatively little hardware and no additional hardware is needed for multiple-pulse detection. The detection of spread spectrum communications presents no special problem.

Figure 3. Radiometer.

Although the radiometer is optimum if we model the signal as a stationary Gaussian process, it is intuitively clear that this receiver is a reasonable configuration for determining the presence of unknown deterministic signals. We now give a performance analysis of the detector, assuming a deterministic signal. The original analysis was done by Urkowitz.[3]

The output of the bandpass filter in figure 3 is $y(t) = s(t) + n(t)$, where $s(t)$ is a deterministic signal and $n(t)$ is Gaussian noise. If the bandpass filter has center frequency f_c and bandwidth W, the deterministic signal can be represented as

$$s(t) = s_c(t) \cos \omega_c t - s_s(t) \sin \omega_c t \ , \qquad (7)$$

where $\omega_c = 2\pi f_c$. Since the spectrum of $s(t)$ is confined within the filter bandwidth, $s_c(t)$ and $s_s(t)$ have frequency components confined to

---

[2] *H. L. Van Trees, Detection, Estimation, and Modulation Theory, III, John Wiley and Sons, Inc., New York (1971).*

[3] *H. Urkowitz, Energy Detection of Unknown Deterministic Signals, Proc. IEEE, 55 (April 1967), 523.*

the band $|f| < W/2$. The Gaussian noise emerging from the bandpass filter can be represented in terms of quadrature components as[4]

$$n(t) = n_c(t) \cos \omega_c t - n_s(t) \sin \omega_c t \quad . \tag{8}$$

If $n(t)$ is filtered white noise of spectral density $N_0/2$, then $n_c(t)$ and $n_s(t)$ have flat power spectral densities, each equal to N_0 over $|f| < W/2$.

As shown in figure 3, the input to the comparator is

$$V(t) = \int_{t-T}^{t} y^2(\tau)\, d\tau \ , \tag{9}$$

where the integration interval is equal to the observation interval, T.

The comparator output may be sampled or continuously fed to a processor. We next determine the probabilities of false alarm and detection associated with V(t) at a fixed time. For convenience, we normalize the test statistic to

$$V = \frac{2}{N_0} \int_0^T y^2(t)\, dt \ . \tag{10}$$

Substituting equations (7) and (8) and assuming that $f_c T >> 1$, $f_c >> W$, we obtain the approximation

$$V = \frac{1}{N_0} \int_0^T \left[s_c(t) + n_c(t) \right]^2 dt$$

$$+ \frac{1}{N_0} \int_0^T \left[s_s(t) + n_s(t) \right]^2 dt \quad . \tag{11}$$

From the sampling theorems for deterministic and stochastic processes,[5] respectively, we obtain expressions that facilitate a statistical performance analysis. After an appropriate choice of time origin, we may write

---

[4] *R. E. Ziemer and W. H. Tranter, Systems, Modulation and Noise, Houghton Mifflin Co., New York (1976).*

[5] *A. Papoulis, Signal Analysis, McGraw-Hill Book Co., New York (1977).*

$$s_c(t) = \sum_{i=-\infty}^{\infty} s_c\left(\frac{i}{W}\right) \text{sinc } (Wt - i) , \tag{12}$$

$$s_s(t) = \sum_{i=-\infty}^{\infty} s_s\left(\frac{i}{W}\right) \text{sinc } (Wt - i) , \tag{13}$$

$$n_c(t) = \sum_{i=-\infty}^{\infty} n_c\left(\frac{i}{W}\right) \text{sinc } (Wt - i) , \tag{14}$$

$$n_s(t) = \sum_{i=-\infty}^{\infty} n_s\left(\frac{i}{W}\right) \text{sinc } (Wt - i) , \tag{15}$$

where sinc $x = \sin \pi x/\pi x$. We make the following approximations, based upon the known properties of the sinc function:

$$\int_0^T \text{sinc } (Wt - i) \text{ sinc } (Wt - j)\, dt \simeq 0 , \quad i \neq j , \tag{16}$$

$$\int_0^T \text{sinc}^2 (Wt - i)\, dt \simeq \int_{-\infty}^{\infty} \text{sinc}^2 (Wt - i)\, dt = \frac{1}{W} , \quad 0 < i \leq TW , \tag{17}$$

$$\int_0^T \text{sinc}^2 (Wt - i)\, dt \simeq 0 , \quad i \leq 0 \text{ or } i > TW . \tag{18}$$

The error introduced by each integral approximation is bounded by 1/2W. Assuming that $TW \geq 1$, the error introduced by equation (18) at $i = 0$ is nearly 1/2W. For other values of i, except possibly $i = TW$, the errors caused by the approximations are much less than 1/2W and decrease as TW increases. Substituting equations (12) to (18) into equation (11), we obtain

$$V = \frac{1}{N_0 W} \sum_{i=1}^{\gamma} \left[s_c\left(\frac{i}{W}\right) + n_c\left(\frac{i}{W}\right) \right]^2$$

$$+ \frac{1}{N_0 W} \sum_{i=1}^{\gamma} \left[s_s\left(\frac{i}{W}\right) + n_s\left(\frac{i}{W}\right) \right]^2 , \tag{19}$$

where γ is the largest integer less than or equal to TW. In view of the approximations made, this equation becomes an increasingly accurate approximation of equation (11) as γ increases. It is always assumed that $\gamma \geq 1$.

We assume that the bandpass filter has a transfer function that is rectangular about f_c. Since n(t) has a power spectral density that is symmetrical about f_c, $n_c(t)$ and $n_s(t)$ are independent Gaussian processes.[4] Thus, $n_c(i/W)$ and $n_s(j/W)$ are independent Gaussian random variables. The power spectral densities of both $n_c(t)$ and $n_s(t)$ are $S(f) = N_0$ for $|f| < W/2$ and $S(f) = 0$ otherwise. The associated autocorrelation function is

$$R(\tau) = N_0 W \operatorname{sinc} W\tau \ . \tag{20}$$

This expression indicates that $n_c(i/W)$ is statistically independent of $n_c(j/W)$, $i \neq j$, and similarly for $n_s(i/W)$ and $n_s(j/W)$. If n(t) is assumed to be zero-mean, so are $n_c(i/W)$ and $n_s(i/W)$. Using these facts, we rewrite equation (19) as

$$V = \sum_{i=1}^{\gamma} a_i^2 + \sum_{i=1}^{\gamma} b_i^2 \ , \tag{21}$$

where the a_i's and the b_i's are statistically independent Gaussian random variables with unit variances and means

$$m_{1i} = E[a_i] = \frac{1}{(N_0 W)^{1/2}} s_c\left(\frac{i}{W}\right), \tag{22}$$

$$m_{2i} = E[b_i] = \frac{1}{(N_0 W)^{1/2}} s_s\left(\frac{i}{W}\right) \ . \tag{23}$$

The first sum in equation (21) has a noncentral χ^2 distribution[1] with γ degrees of freedom and a noncentral parameter $\lambda_1 = \sum m_{1i}^2$. Similarly, the second sum has a noncentral χ^2 distribution with γ degrees of freedom and a noncentral parameter $\lambda_2 = \sum m_{2i}^2$. Since the two

---

[1] *A. Whalen, Detection of Signals in Noise, Academic Press, Inc., New York (1971).*

[4] *R. E. Ziemer and W. H. Tranter, Systems, Modulation and Noise, Houghton Mifflin Co., New York (1976).*

χ^2 variables are independent, V has a noncentral χ^2 distribution with 2γ degrees of freedom and noncentral parameter $\lambda = \lambda_1 + \lambda_2$. Thus,

$$\lambda = \frac{1}{N_0 W} \sum_{i=1}^{\gamma} s_c^2\left(\frac{i}{W}\right) + \frac{1}{N_0 W} \sum_{i=1}^{\gamma} s_s^2\left(\frac{i}{W}\right)$$

$$\simeq \frac{1}{N_0} \int_0^T \left[s_c^2(t) + s_s^2(t)\right] \, dt$$

$$\simeq \frac{2}{N_0} \int_0^T s^2(t) \, dt \, . \tag{24}$$

In terms of the signal energy, E, we have the approximation

$$\lambda = \frac{2E}{N_0} \, . \tag{25}$$

By straightforward calculations using the statistics of Gaussian variates, the mean and the variance of V are determined to be

$$E[V] = \lambda + 2\gamma \, , \tag{26}$$

$$VAR(V) = 4\lambda + 4\gamma \, . \tag{27}$$

By using the known probability density functions for a noncentral χ^2 random variable, the false alarm and detection probabilities can be expressed as integrals. In the absence of a signal, the χ^2 probability density function for V is

$$p_0(v) = \frac{1}{2^{\gamma}\Gamma(\gamma)} v^{\gamma-1} e^{-v/2} \, , \qquad v \leq 0 \tag{28}$$

$$p_0(v) = 0 \, , \qquad v < 0$$

where $\Gamma(x)$ is the gamma function. The false alarm probability is

$$P_F = \int_{V_T}^{\infty} p_0(v) \, dv \, . \tag{29}$$

If the signal is present, the χ^2 probability density function for V is

$$p_1(v) = \frac{1}{2}\left(\frac{v}{\lambda}\right)^{(\gamma-1)/2} \exp\left(-\frac{v+\lambda}{2}\right) I_{\gamma-1}\left(\sqrt{v\lambda}\right), \quad v \geq 0,$$

$$p_1(v) = 0, \quad v < 0, \tag{30}$$

where $I_n(x)$ is the modified Bessel function of the first kind and order n. The probability of detection is

$$P_D = \int_{V_T}^{\infty} p_1(v)\, dv . \tag{31}$$

Numerous schemes for evaluating P_F and P_D have been proposed in the literature.[1,3]

We are particularly interested in the case in which TW is large since this case includes the interception of spread spectrum communications. When TW is large, $\gamma \simeq TW$, and the central limit theorem indicates that V is approximated by a Gaussian variate. Using equations (26) and (27) with $\lambda = 0$ and equation (29) with a Gaussian density for $p_0(v)$, we obtain

$$P_F = \frac{1}{(8\pi TW)^{1/2}} \int_{V_T}^{\infty} \exp\left[-\frac{(v-2TW)^2}{8TW}\right] dv$$

$$= \frac{1}{2}\,\mathrm{erfc}\left[\frac{V_T - 2TW}{(8TW)^{1/2}}\right] . \tag{32}$$

Similarly, we obtain

$$P_D = \frac{1}{2}\,\mathrm{erfc}\left[\frac{V_T - 2TW - \lambda}{(8TW + 8\lambda)^{1/2}}\right] . \tag{33}$$

---

[1] *A. Whalen, Detection of Signals in Noise, Academic Press, Inc., New York (1971).*

[3] *H. Urkowitz, Energy Detection of Unknown Deterministic Signals, Proc. IEEE, 55 (April 1967), 523.*

Combining equations (4), (5), (32), and (33) gives

$$(8TW + 8\lambda)^{1/2}\,\xi = (8TW)^{1/2}\,\beta - \lambda \ . \tag{34}$$

We can solve this equation to determine the value of E/N_0 necessary to achieve specified values of P_F and P_D. Solving for λ and using equation (25), we obtain

$$\frac{E}{N_0} = 2\xi^2 + \beta(2TW)^{1/2} - \xi\left[2TW + 4\xi^2 + 2\beta(8TW)^{1/2}\right]^{1/2} . \tag{35}$$

If we assume that $TW >> \beta^2$ and $TW >> \xi^2$, then further simplification is possible. The result is

$$\frac{E}{N_0} = (2TW)^{1/2}\,(\beta - \xi) \ , \qquad TW >> \max\left(\beta^2,\ \xi^2\right) . \tag{36}$$

Comparing equations (36) and (6), we see that the disparity in performance between the radiometer and the matched filter increases with TW. Equation (36) indicates that detection difficulties increase as the intercepted signal spectum is spread.

Denoting the intercepted signal power by R_s and the signal duration by T_1, the intercepted power necessary to achieve specified values of P_F and P_D is

$$R_s = N_0\,\frac{(2TW)^{1/2}}{T_1}\,(\beta - \xi) \ , \quad T_1 < T \ , \quad TW >> \max\left(\beta^2,\ \xi^2\right) ,$$

$$R_s = N_0\left(\frac{2W}{T}\right)^{1/2}(\beta - \xi) \ , \quad T_1 \geq T \ , \quad TW >> \max\left(\beta^2,\ \xi^2\right) . \tag{37}$$

As long as $T_1 \geq T$, this equation indicates that increasing the observation interval decreases the required power. However, if $T_1 < T$, an increase in the observation interval increases the required power.

If the outputs of N_r independent radiometers are averaged, a straightforward calculation shows that the required R_s can be reduced by a factor of $N_r^{-1/2}$.

2.2 Channelized Radiometer

A channelized radiometer forms when M radiometers are inserted in the branches of figure 2, as depicted in figure 4(a). Each block labeled radiometer contains a bandpass filter of bandwidth W/M, a squaring device, and an integrator, but no comparator. Let T_s denote the sampling interval, which is the observation interval of the constituent radiometers. To avoid processing extraneous noise, the arrival time of the signal to be intercepted may be estimated by additional hardware. The sampling interval may equal or be somewhat less than the minimum expected signal duration in a channel. To increase effectiveness against frequency hopping or multiple frequency-shift keying (MFSK), the processor examines N consecutive comparator outputs and determines that a signal is present if r of these outputs correspond to comparator inputs that exceed the threshold. For example, if N is odd, a majority decision rule requires $r = (N + 1)/2$. The effective observation interval of the channelized radiometer, given by $T = NT_s$, should usually be less than the minimum expected message duration. If it is known that the intercepted signal is narrowband, we can set N = 1. If the presence of more than one signal is to be verified, it is desirable to employ an array of radiometers of the form of figure 3 with the comparator outputs feeding into a processor that analyzes the activity of individual channels, as shown in figure 4(b). In this configuration, N = 1 and each bandpass filter has a bandwidth of W/M.

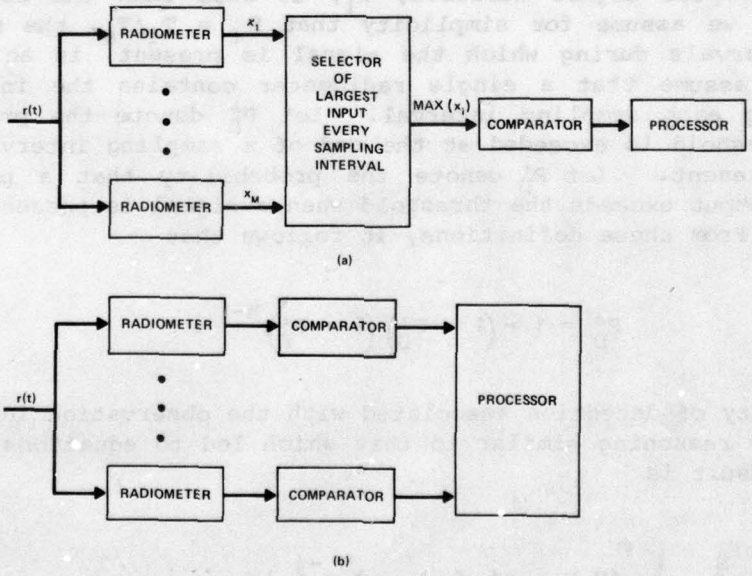

Figure 4. Channelized radiometers (a) for detection of presence of hostile communications and (b) for simultaneous detection of multiple signals.

To simplify the analysis of the interception of a single signal, we assume that the N sets of radiometer outputs are statistically independent. If P'_F is the probability that a particular radiometer output exceeds the threshold when no signal is present, then the probability that none of the radiometer outputs exceeds the threshold is $(1 - P'_F)^M$, assuming that the channel noises are statistically independent. The probability that exactly i out of N comparator inputs exceeds the threshold is

$$P(i, N) = \binom{N}{i} \left[1 - \left(1 - P'_F\right)^M\right]^i \left(1 - P'_F\right)^{M(N-i)} , \quad i \leq N ,$$

$$P(i, N) = 0 , \quad i > N . \tag{38}$$

It follows that the probability of false alarm associated with the observation interval is

$$P_F = \sum_{i=r}^{N} P(i, N) . \tag{39}$$

If the intercepted signal duration, T_1, is less than the observation interval, T, we assume for simplicity that $N_1 = T_1/T_s$, the number of sampling intervals during which the signal is present, is an integer. Further, we assume that a single radiometer contains the intercepted signal during each sampling interval. Let P''_D denote the probability that the threshold is exceeded at the end of a sampling interval when a signal is present. Let P'_D denote the probability that a particular radiometer output exceeds the threshold when a signal is present in that radiometer. From these definitions, it follows that

$$P''_D = 1 - \left(1 - P'_D\right)\left(1 - P'_F\right)^{M-1} . \tag{40}$$

The probability of detection associated with the observation interval is determined by reasoning similar to that which led to equations (38) and (39). The result is

$$P_D = \sum_{i=r}^{N} \sum_{j=0}^{i} \binom{N_1}{j} \left(P''_D\right)^j \left(1 - P''_D\right)^{N_1 - j} P\left(i - j, \; N - N_1\right) . \tag{41}$$

To compare the channelized radiometer with a single wideband radiometer, we assume that $N = N_1$ and that the energy of the intercepted signal is equally divided among the N sampling intervals. Since the total receiver bandwidth is W, the bandwidth of each constituent radiometer is $W_s = W/M$. Thus, for large values of $T_s W_s$, P_F' and P_D' are given by equations (32) and (33) with $W_s = W/M$ substituted for W, $T_s = T/N$ substituted for T, and $\lambda_s = \lambda/N$ substituted for λ. We have

$$P_F' = \frac{1}{2} \operatorname{erfc} \left[\frac{MNV_T - 2TW}{(8TWMN)^{1/2}} \right], \tag{42}$$

$$P_D' = \frac{1}{2} \operatorname{erfc} \left[\frac{MNV_T - 2TW - \lambda M}{(8TWMN + 8\lambda M^2 N)^{1/2}} \right] . \tag{43}$$

We define

$$\beta_1 = \operatorname{erfc}^{-1} \left(2P_F' \right) , \tag{44}$$

$$\xi_1 = \operatorname{erfc}^{-1} \left(2P_D' \right) . \tag{45}$$

If P_F and P_D are specified, we solve equations (38) to (41) for P_F' and P_D'. Using equations (42) to (45), we perform a calculation analogous to that used in deriving equation (37). The result is that the required R_s for detection with specified values of P_F and P_D is

$$R_s \simeq N_0 \left(\frac{2WN}{MT} \right)^{1/2} \left(\beta_1 - \xi_1 \right) , \quad T_1 \geq T, \; TW >> MN \max \left(\beta_1^2 , \xi_1^2 \right) . \tag{46}$$

If a frequency-hopping signal is to be intercepted, the parameter N is proportional to the hopping rate. Thus, equation (46) indicates that the required power is proportional to the square root of the hopping rate. If $M >> N$, the channelized radiometer requires less power than a wideband radiometer with the same values of T and W. If we set $N = 1$ and attempt to intercept a frequency-hopping signal by processing each hop, then T must be decreased as the hopping rate increases.

Suppose that the energy is concentrated in a narrow bandwidth during the observation interval and that the bandwidths of the radiometers are sufficiently wide so that the energy enters a single radiometer. Then we may take $r = N = N_1 = 1$. Equations (39) and (41) reduce to

$$P_F = 1 - \left(1 - P_F'\right)^M , \tag{47}$$

$$P_D = 1 - \left(1 - P_D'\right)\left(1 - P_F'\right)^{M-1} . \tag{48}$$

The required value of R_s for detection is determined by the usual method to be

$$R_s \simeq N_0 \left(\frac{2W}{MT}\right)^{1/2} \left(\beta_1 - \xi_1\right) , \quad T_1 \geq T, \quad TW >> M \max\left(\beta_1^2, \xi_1^2\right) , \tag{49}$$

where

$$\beta_1 = \operatorname{erfc}^{-1}\left[2 - 2\left(1 - P_F\right)^{1/M}\right] , \tag{50}$$

$$\xi_1 = \operatorname{erfc}^{-1}\left[2 - \frac{2\left(1 - P_D\right)}{\left(1 - P_F\right)^{1-1/M}}\right] . \tag{51}$$

Thus, the required power falls approximately as the square root of the number of channels.

To determine P_F' and P_D' when equations (42) and (43) do not apply, we assume that the intercepted signal energy is equally divided among the N_1 sampling intervals. We use equations (28) to (31) with $\lambda_s = \lambda/N_1$ substituted for λ and η, the largest integer less than or equal to $T_s W_s$, substituted for γ. The results are

$$P_F' = \frac{1}{2^{\eta}\Gamma(\eta)} \int_{V_T}^{\infty} v^{\eta-1} \exp\left(-\frac{v}{2}\right) dv , \tag{52}$$

$$P'_D = \frac{1}{2} \int_{V_T}^{\infty} \left(\frac{v}{\lambda_s}\right)^{(\eta - 1)/2} \exp\left(-\frac{v + \lambda_s}{2}\right) I_{\eta-1}\left(\sqrt{v\lambda_s}\right) dv \quad . \qquad (53)$$

By numerical methods, this pair of equations can be solved simultaneously to eliminate V_T and express $\lambda = N_1\lambda_s$ as a function of P'_F and P'_D. If we solve equations (38) to (41) for P'_F and P'_D in terms of P_F and P_D, then we can obtain an equation for λ in terms of P_F and P_D. From this equation, we finally obtain the required value of R_s necessary to achieve specified values of P_F and P_D.

The channelized radiometer has been shown to be relatively effective against conventional and frequency-hopping communications. It is also useful against pseudonoise spread spectrum communications if preliminary processing is used to produce a signal with a narrow bandwidth (sect. 3).

2.3 Cross Correlator

The ideal correlator of figure 1 can be approximated if the signal is intercepted at two spatially separated antennas. The cross-correlation function of the two antenna outputs is estimated for various relative arrival times, and the peak value of this function is applied to a comparator. Figure 5 is a block diagram of a realization employing the discrete Fourier transform (DFT). One way to implement the DFT is to use a digital filter and the fast Fourier transform algorithm. An alternative implementation is to use the chirp Z-transform algorithm and charge-coupled devices. An analog realization of the cross-correlation function that is similar to the configuration of figure 5 can be accomplished with dispersive filters providing Fourier transforms (sect. 3.6). Elegant realizations are possible with acousto-optical devices.[6]

Figure 5a depicts the initial processing of each antenna output. After passage through the bandpass filter of bandwidth W, the intercepted waveform, $r(t) = s(t) + n(t)$, can be represented as

$$r(t) = r_c(t) \cos \omega_c t - r_s(t) \sin \omega_c t \quad , \qquad (54)$$

where the quadrature components, $r_c(t)$ and $r_s(t)$, are confined to the band $|f| \leq W/2$. If the two lowpass filters have bandwidths W/2 and $f_c = \omega_c/2\pi > W/2$, then $r_c(t)$ and $r_s(t)$ are extracted by the operations shown in figure 5(a). Analog-to-digital converters produce the discrete sequences $r_c(i/W)$ and $r_s(i/W)$.

[6] *R. A. Sprague, A Review of Acousto-optic Signal Correlators, Optical Engineering, 16 (September 1977), 467.*

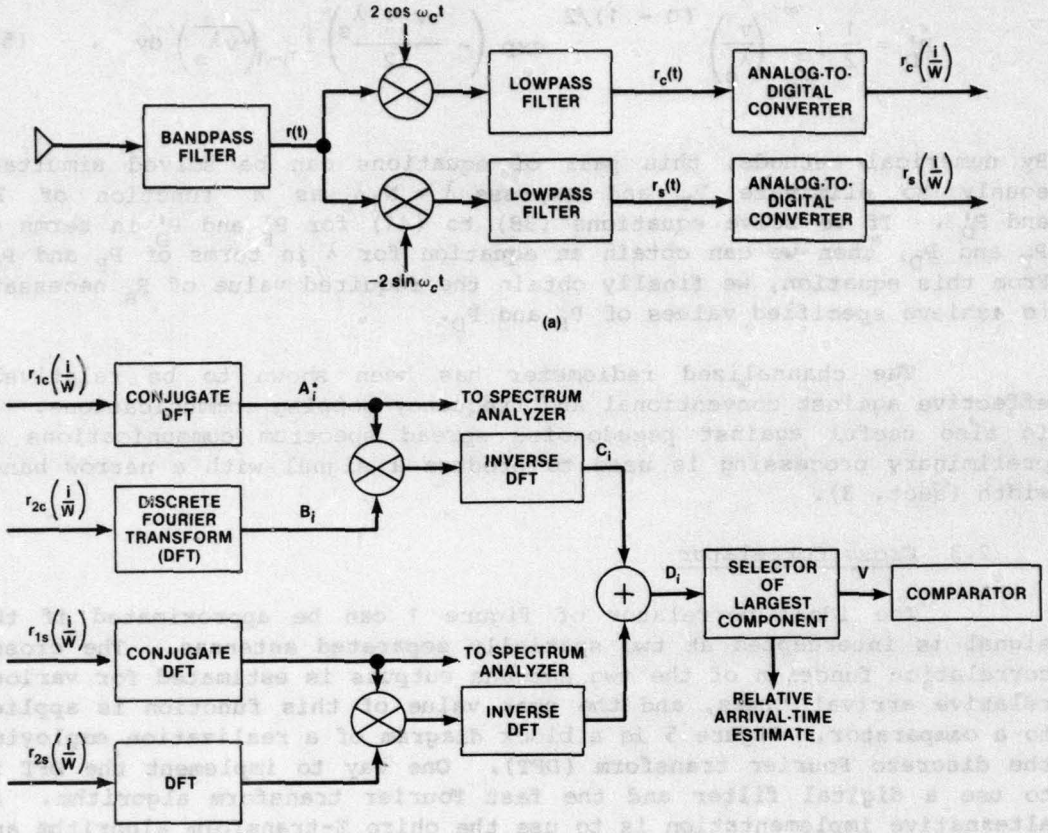

Figure 5. Cross correlator: (a) initial processing of each antenna output and (b) final processing.

We regard one of the antennas as a reference and denote its output by the subscript 1. In terms of the signal and the noise, we have

$$r_1(t) = s(t) + n_1(t) \quad , \tag{55}$$

$$r_{1c}(t) = s_c(t) + n_{1c}(t) \quad , \tag{56}$$

$$r_{1s}(t) = s_s(t) + n_{1s}(t) \quad . \tag{57}$$

Denoting the output of the other antenna by the subscript 2, we have

$$r_2(t) = s\left(t - T_r\right) + n_2'(t) \quad , \tag{58}$$

$$r_{2c}(t) = s_c\left(t - T_r\right) + n_{2c}'(t) \quad , \tag{59}$$

$$r_{2s}(t) = s_s\left(t - T_r\right) + n_{2s}'(t) \quad , \tag{60}$$

where T_r is the arrival time of the intercepted signal at this antenna output relative to the arrival time at the reference antenna output. By inserting a sufficiently long delay before this antenna output, we ensure that $T_r \geq 0$. It is convenient to use the notation

$$a_i = r_{1c}\left(\frac{i + 1}{W}\right) \quad , \quad i = 0, 1, \ldots, \gamma - 1, \tag{61}$$

$$b_i = r_{2c}\left(\frac{i + 1}{W}\right) \quad , \quad i = 0, 1, \ldots, \gamma - 1$$

for two of the discrete sequences observed during the interval T. We form sequences with $K = \gamma + N_c - 1$ points by augmenting the a_i and b_i with $N_c - 1$ zeros, where $N_c \leq \gamma$. As indicated in figure 5(b), the conjugate DFT of a_i is calculated, giving

$$A_i^* = \sum_{n=0}^{K-1} a_n \Omega_K^{-in} \quad , \quad i = 0, 1, \ldots, K - 1, \tag{62}$$

where $\Omega_K = \exp(-j2\pi/K)$ and $j = \sqrt{-1}$. Similarly, the DFT of b_i is

$$B_i = \sum_{n=0}^{K-1} b_n \Omega_K^{in} \quad , \quad i = 0, 1, \ldots, K - 1 \quad . \tag{63}$$

The inverse DFT of the product $A_i^* B_i$ for $0 \leq N_c - 1$ is

$$C_i = \frac{1}{K} \sum_{n=0}^{K-1} A_n^* B_n \Omega_K^{-in}$$

$$= \frac{1}{K} \sum_{m=0}^{K-1} \sum_{k=0}^{K-1} a_m b_k \sum_{n=0}^{K-1} \Omega_K^{n(-m+k-i)}$$

$$= \sum_{k=0}^{\gamma-1} \sum_{m=0}^{\gamma-1} a_m b_k \delta_{m,k-i} = \sum_{k=i}^{\gamma-1} a_{k-i} b_k \quad , \tag{64}$$

where δ_{ik} is the Kronecker delta. From the original definitions and equations similar to equations (12) to (18), we obtain for $i \ll TW$,

$$C_i = \sum_{k=i}^{\gamma-1} r_{1c}\left(\frac{k+1-i}{W}\right) r_{2c}\left(\frac{k+1}{W}\right)$$

$$\simeq W \int_{i/W}^{T} r_{1c}\left(t - \frac{i}{W}\right) r_{2c}(t)\, dt \quad . \tag{65}$$

This sequence is the output of one of the inverse DFT operations shown in figure 5(b). An analogous expression can be written for the output of the other inverse DFT operation. The addition of the two sequences produces a sequence proportional to

$$D_i = \int_{i/W}^{T} \left[r_{1c}\left(t - \frac{i}{W}\right) r_{2c}(t) + r_{1s}\left(t - \frac{i}{W}\right) r_{2s}(t) \right] dt \quad . \tag{66}$$

If $f_c \gg W$, then expansions similar to equation (54) lead to the approximation

$$D_i \simeq \int_{i/W} 2 r_1\left(t - \frac{i}{W}\right) r_2(t)\, dt \, , \; i = 0, 1, \ldots, N_c - 1 \, . \tag{67}$$

To interpret the next operation in figure 5(b), we initially assume that no noise is present. In this case, equations (55) and (58) yield

$$D_i = \int_{i/W}^{T} 2s\left(t - \frac{i}{W}\right) s\left(t - T_r\right) dt \ , \quad i = 0, 1, \ldots, N_c - 1 \ . \tag{68}$$

Thus, the D_i provide sampled values of an approximation of the autocorrelation function of s(t). Let i_0 denote the index that corresponds to the largest D_i. Assuming that the approximation is adequate and that the autocorrelation function has a sharp peak, i_0 is the index closest to the value $T_r W$. When noise is present, this statement may not be true; however, to proceed with the analysis, we assume that it is. Note that T_r can be estimated as i_0/W. This estimate can be used for direction finding (sect. 4.2).

Assuming that the largest D_i has index $i_0 = T_r W \leq N_c - 1$ and normalizing, the input to the comparator in figure 5(b) is the test statistic

$$\begin{aligned} V &= \frac{2}{N_0} \int_{T_r}^{T} r_1\left(t - T_r\right) r_2(t)\, dt \\ &= \frac{2}{N_0} \int_{0}^{T-T_r} r_1(t) r_2\left(t + T_r\right)\, dt \ . \end{aligned} \tag{69}$$

Substituting equations (55) and (58) and defining $n_2(t) = n_2'(t + T_r)$ and $T_a = T - T_r$, we get

$$V = \frac{2}{N_0} \int_{0}^{T_a} \left[s(t) + n_1(t)\right]\left[s(t) + n_2(t)\right] dt \ . \tag{70}$$

In the usual manner, we obtain the series expansion

$$\begin{aligned} V = &\frac{1}{N_0 W} \sum_{i=1}^{\gamma_a} \left[s_c\left(\frac{i}{W}\right) + n_{1c}\left(\frac{i}{W}\right)\right]\left[s_c\left(\frac{i}{W}\right) + n_{2c}\left(\frac{i}{W}\right)\right] \\ &+ \frac{1}{N_0 W} \sum_{i=1}^{\gamma_a} \left[s_s\left(\frac{i}{W}\right) + n_{1s}\left(\frac{i}{W}\right)\right]\left[s_s\left(\frac{i}{W}\right) + n_{2s}\left(\frac{i}{W}\right)\right] \ , \end{aligned} \tag{71}$$

where γ_a is the largest integer less than or equal to T_aW. Assuming that $n_1(t)$ and $n_2(t)$ are statistically independent, zero-mean, Gaussian processes, a straightforward calculation yields

$$E[V] = \lambda_a \quad , \tag{72}$$

$$VAR(V) = 2\lambda_a + 2\gamma_a \quad , \tag{73}$$

where $\lambda_a = 2E_a/N_0$ and E_a is the energy in interval T_a.

For large values of T_aW, the test statistic is approximately normally distributed. It follows that

$$P_D = \frac{1}{2} \operatorname{erfc} \left[\frac{V_T - \lambda_a}{\left(4T_aW + 4\lambda_a\right)^{1/2}} \right] \quad . \tag{74}$$

According to equation (67), the cross-correlation function is computed for N_c sample values. However, the maximum possible value of T_r may be such that only $N_c << \gamma$ sample values need to be computed to obtain V. When no signal is present, a false alarm occurs if any of the N_c estimated cross-correlation values exceeds the threshold. If N_c is sufficiently small, it is reasonable to assume that each estimated value has approximately the same probability, denoted by P_F', of exceeding the threshold. This assumption implies the approximation,

$$P_F = 1 - \left(1 - P_F'\right)^{N_c} \quad , \tag{75}$$

where P_F' is the probability that

$$V = \int_0^{T_a} n_1(t)\, n_2(t)\, dt \tag{76}$$

exceeds the threshold. The mean and the variance of equation (76) are given by equations (72) and (73) with $\lambda_a = 0$. For large values of T_aW, we obtain

$$P'_F = \operatorname{erfc}\left[\frac{V_T}{\left(4T_aW\right)^{1/2}}\right] . \tag{77}$$

Equations (44) and (75) yield

$$\beta_1 = \operatorname{erfc}^{-1}\left[2 - 2\left(1 - P_F\right)^{1/N_c}\right] \tag{78}$$

We obtain in the usual manner the required R_s to detect a signal with specified values of P_F and P_D. The result is

$$R_s \simeq N_0 \frac{\left(T_aW\right)^{1/2}}{T_1}\left(\beta_1 - \xi\right) , \quad T_1 < T_a , \quad T_aW >> \max\left(\beta_1^2, \xi^2\right) ,$$

$$R_s \simeq N_0\left(\frac{W}{T_a}\right)^{1/2}\left(\beta_1 - \xi\right), \quad T_1 \geq T_a , \quad T_aW >> \max\left(\beta_1^2, \xi^2\right) , \tag{79}$$

where T_1 is the signal duration.

Comparison with equation (37) indicates that the cross correlator can give a theoretical improvement of approximately 1.5 dB over a single wideband radiometer. Taking into account the approximations made to derive equation (79), it is possible that in practice the cross correlator provides no improvement at all. A comparison of figures 3 and 5 indicates that the implementation of the cross correlator entails considerably more hardware than the implementation of a wideband radiometer. However, as discussed in subsequent sections, the cross correlator requires little additional hardware to provide frequency estimation and direction finding.

The channelized cross correlator is an array of M cross correlators, each of which has a bandwidth of W/M. The outputs of the array are applied to a processor. Analogously to the channelized radiometer, the channelized cross correlator may be preferable to a single wideband cross correlator when the hostile communications are narrowband or when two or more simultaneous signals are to be intercepted.

Equations (37) and (79) indicate that increasing the bandwidth of a frequency-hopping system degrades the performance against a single signal of both the wideband cross correlator and the wideband radiometer. However, neither of these receivers is sensitive to the hopping

rate. Increasing the hopping rate makes the practical design of a channelized receiver more difficult and degrades its performance. If the rate is sufficiently high, the channelized receiver may have to be abandoned in favor of a wideband receiver.

3. FREQUENCY ESTIMATION

The immediate purpose of a frequency estimation system is to determine the center frequency and possibly the spectral shape of an intercepted signal. If a frequency-hopping signal is intercepted, the purpose is to determine each hopping frequency or at least the frequency range over which the hopping occurs.

Although not desirable for some purposes, such as message analysis, preliminary processing of pseudonoise spread-spectrum communications is desirable before estimation of the center frequency is attempted. An intercepted binary pseudonoise signal has the form

$$s(t) = Am(t)p(t) \cos \omega_0 t \quad , \tag{80}$$

where A is the amplitude, ω_0 is the center frequency, m(t) is the binary message sequence, and p(t) is a binary pseudorandom sequence. Both $m(t)$ and $p(t)$ take the values +1 or -1. Suppose s(t) enters a wideband receiver and is squared. Since $m^2 = p^2 = 1$, the output of the squaring device is proportional to

$$s^2(t) = A^2 \cos^2 \omega_0 t = \frac{A^2}{2} + \frac{A^2}{2} \cos 2 \omega_0 t \quad . \tag{81}$$

The double-frequency term is now a pure pulsed sinusoid. Its frequency and, thus, the center frequency of s(t) can be estimated by the systems described in this section. The same preliminary processing is useful against phase-shift keyed communications.

3.1 Channelized Receiver

Estimation theory leads to the receiver of figure 2 for frequency estimation, assuming that the arrival time and the signal waveform, except for a uniformly distributed phase angle, are known.[1] After the largest output is selected, the unknown frequency is estimated as the center frequency of the filter producing the largest output. A practical approximation to this receiver is the channelized radiometer of figure 4.

[1] *A. Whalen, Detection of Signals in Noise, Academic Press, Inc., New York (1971).*

Suppose we desire a frequency resolution of Δ, where Δ is not less than the Cramer-Rao bound.[1] If the entire range of reconnoitered frequencies is W, then each filter must have bandwidth 2Δ and $M = W/2\Delta$ is the number of required filters to attain the desired accuracy. If the intercepted signal has duration T, then each filter must have bandwidth 2/T for most of the signal energy to pass through it. Thus, we have

$$\Delta = \frac{1}{T} \quad . \tag{82}$$

If $M \geq 6$, the number of required filters can be reduced by arranging the filters in successive stages, as shown in figure 6 for the case in which each stage has the same number of filters. After an intercepted signal passes through the first filter bank, its frequency is theoretically known within an accuracy of $\Delta_1 = W/2M_s$, where M_s is the number of filters in each stage and $2\Delta_1$ is the bandwidth of the first stage filters. A bank of mixers ensures that the filter outputs are shifted in frequency so that the input to the second stage has a frequency between $f_{11} - f_{c1} - \Delta_1$ and $f_{11} - f_{c1} + \Delta_1$, where f_{11} is the center frequency of the top filter in the first bank and f_{c1} is the frequency of a local oscillator. After the input passes through the second filter bank, the frequency is known within an accuracy $\Delta_2 = \Delta_1/M_s$, and so on. If N_s stages of M_s filters each are employed, then an accuracy of Δ is attained if

$$M_s^{N_s} = \frac{W}{2\Delta} \tag{83}$$

The total number of filters required is $M_s N_s$. Disadvantages of the channelized receiver of figure 6 relative to that of figure 4 are the increased processing time required for frequency estimation, the reduced amount of noise and interference filtering, and the ambiguities that arise when more than one signal is intercepted.

It is not necessary that each stage have the same number of filters. However, if N_s, W, and Δ are fixed, it can easily be shown, using Lagrange multipliers, that the total number of filters is minimized if each stage has approximately the same number of filters (exactly the same number if an integer M_s exists that satisfies eq [83]). If each stage has the same number of filters and W and Δ are fixed, it can be shown that the total number of filters is minimized if each stage has three filters. (Lagrange multipliers yield $M_s = e$, but M_s must be an integer.)

---

[1] *A. Whalen, Detection of Signals in Noise, Academic Press, Inc., New York (1971).*

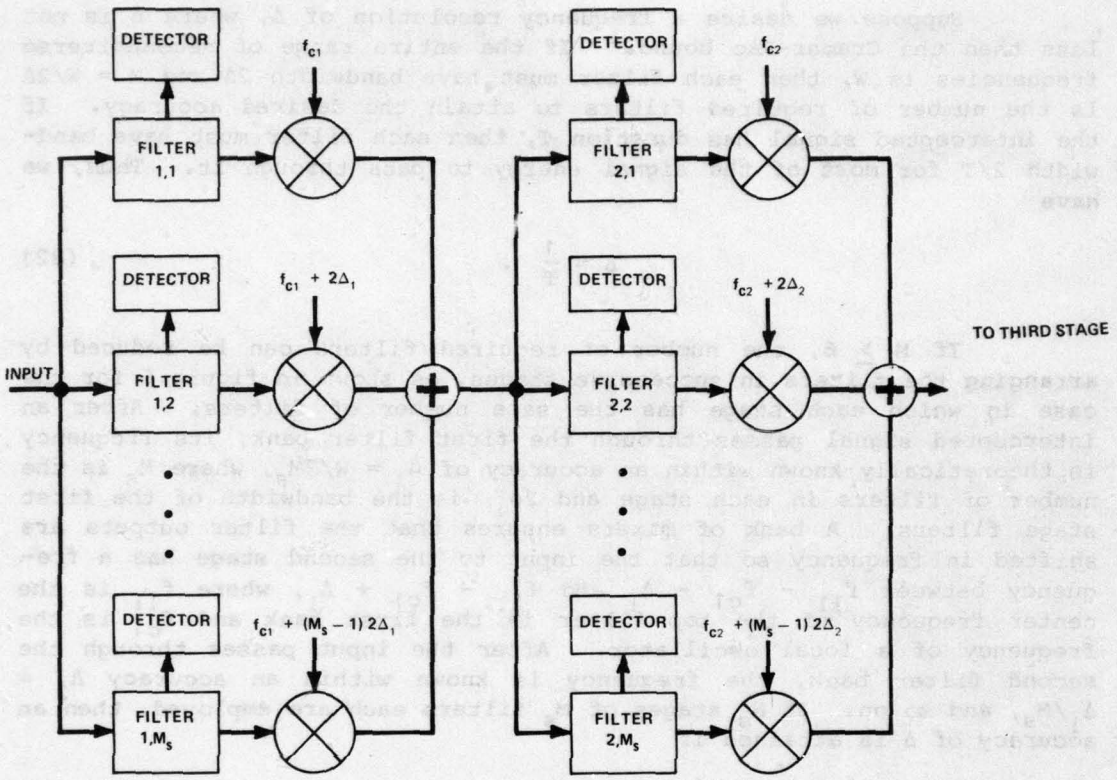

Figure 6. Channelized receiver with filters arranged in successive stages.

Even when minimized, the number of filters and detectors required in a channelized receiver may make this method of frequency estimation expensive. In this case, a limited number of filters can be used to reduce the total bandwidth examined by other frequency estimation devices.

3.2 Spectrum Analysis with Discrete Fourier Transform

The outputs of the two conjugate DFT blocks in figure 5(b) provide a scaled phase-shifted estimate of the intercepted spectrum over the receiver bandwidth. To see how the spectrum is estimated, we first define the truncated waveforms:

$$s'(t) = s(t)q(t) \quad ,$$

$$s'_c(t) = s_c(t)q(t) \quad ,$$

$$s'_s(t) = s_s(t)q(t) \quad , \tag{84}$$

where

$$q(t) = 1 , \quad 0 < t \leq T ,$$

$$q(t) = 0, \quad \text{otherwise} . \tag{85}$$

We denote the Fourier transforms of $s'(t)$, $s'_c(t)$, and $s'_s(t)$ by $S(\omega)$, $S_c(\omega)$, and $S_s(\omega)$, respectively. From equation (7),

$$S(\omega) = \frac{1}{2} S_c\left(\omega - \omega_c\right) + \frac{1}{2} S_c\left(\omega + \omega_c\right)$$

$$- \frac{1}{2j} S_s\left(\omega - \omega_c\right) + \frac{1}{2j} S_s\left(\omega + \omega_c\right) . \tag{86}$$

We are interested in determining $S(\omega)$ for $\omega \geq 0$. If $\omega_c \geq \pi W$, then

$$S(\omega) = \frac{1}{2} S_c\left(\omega - \omega_c\right) - \frac{1}{2j} S_s\left(\omega - \omega_c\right) , \quad \omega \geq 0 , \ \omega_c \geq \pi W . \tag{87}$$

Thus, we can estimate $S(\omega)$ if we first estimate $S_c(\omega)$ and $S_s(\omega)$.

We give the details of the estimation of $S_c(\omega)$; the estimation of $S_s(\omega)$ is similar. For simplicity, we assume $K \simeq TW$. The sample values of $S_c(\omega)$ are related to those of $s'_c(t)$ through the fundamental relation[5]

$$\bar{S}_c(nx) = \frac{2\pi}{Nx} \sum_{m=0}^{N-1} \bar{s}_c\left(m \frac{2\pi}{Nx}\right) \Omega_N^{mn}$$

$$= \frac{2\pi}{Nx} \sum_{m=1}^{N} \bar{s}_c\left(m \frac{2\pi}{Nx}\right) \Omega_N^{mn} , \quad n = 0, 1, \ldots, N - 1 , \tag{88}$$

where $\Omega_N = \exp(-j2\pi/N)$ and

$$\bar{s}_c(my) = \sum_{k=-\infty}^{\infty} s'_c(my + kNy) , \tag{89}$$

$$\bar{S}_c(nx) = \sum_{i=-\infty}^{\infty} S_c(nx + iNx) . \tag{90}$$

We apply these equations with $N = \gamma = TW$, $x = 2\pi/T$, and $y = 1/W$. Since $s_c'(t) = 0$ unless $0 < t \leq T$, equation (89) implies that

$$\bar{s}_c\left(\frac{m}{W}\right) = s_c'\left(\frac{m}{W}\right) = s_c\left(\frac{m}{W}\right) , \quad 1 \leq m \leq TW \quad . \tag{91}$$

Consequently, equation (88) becomes

$$\bar{S}_c\left(n\,\frac{2\pi}{T}\right) = \frac{1}{W} \sum_{m=1}^{TW} s_c\left(\frac{m}{W}\right) \Omega_{TW}^{mn} \quad , \quad n = 0 \, , \; 1 \, , \; \ldots \, , \; TW - 1 \quad . \tag{92}$$

We assume that $S(\omega) \simeq 0$, unless $|\omega - \omega_c| < \pi W$ or $|\omega + \omega_c| < \pi W$. Consequently, $S_c(\omega) \simeq 0$ for $|\omega| \geq \pi W$, and equation (90) yields the approximate result

$$\bar{S}_c\left(n\,\frac{2\pi}{T}\right) = S_c\left(n\,\frac{2\pi}{T}\right) , \quad 0 \leq n \leq TW/2 \quad ,$$

$$\bar{S}_c\left(n\,\frac{2\pi}{T}\right) = S_c\left(n\,\frac{2\pi}{T} - 2\pi W\right) , \quad TW/2 \leq n \leq TW - 1 \quad . \tag{93}$$

Equations (92) and (93) imply that

$$S_c\left(n\,\frac{2\pi}{T}\right) = \frac{1}{W} \sum_{m=1}^{TW} s_c\left(\frac{m}{W}\right) \Omega_{TW}^{mn}, \quad |n| \leq TW/2 \quad . \tag{94}$$

We conclude that, in the presence of noise, a reasonable estimator of the sample values of $S_c(\omega)$ is given by the right side of equation (94) with s_c replaced by r_{1c}. Using equations (61) and (62), we obtain

$$\hat{S}_c\left(n\,\frac{2\pi}{T}\right) = \frac{1}{W} A_n \Omega_{TW}^{n} \quad , \quad 0 \leq n \leq TW/2 \quad ,$$

$$\hat{S}_c\left(n\,\frac{2\pi}{T}\right) = \frac{1}{W} A_{-n}^{*} \Omega_{TW}^{n} \quad , \quad -TW/2 \leq n < 0 \quad . \tag{95}$$

If no noise is present, then $\hat{S}_c(\omega) = S_c(\omega)$ at the sample values. The resolution of $\hat{S}_c(\omega)$ and $\hat{S}_s(\omega)$, the corresponding estimator for $S_s(\omega)$, is primarily determined by the duration of the sample pulse. The resolution is

$$\Delta \simeq \frac{1}{T} \quad . \tag{96}$$

To obtain a more accurate expression for Δ, the effects of the random noise must be evaluated. However, equation (96) is adequate for roughly comparing the frequency estimation potential of the cross correlator with that of competitive systems.

If the frequencies of frequency hopping or MFSK communications are to be successfully estimated, the observation time, T, must be less than the period between frequency changes.

3.3 Acousto-optical Receiver

Spectrum analysis using acousto-optical diffraction has the potential capability for real-time, wideband frequency estimation of many simultaneous signals. The principal components of an acousto-optical spectrum analyzer are shown in figure 7. The diffraction geometry associated with the Bragg cell is illustrated in figure 8. The Bragg cell converts an electronic input at frequency f_0 into a traveling acoustic wave with velocity v_a and wavelength $\Lambda_a = v_a/f_0$. The laser light has wavelength Λ_o in free space and Λ_o/n inside the cell, which has an index of refraction n. According to Bragg's law, the sound wave interacts with the light beam to produce a principal diffracted beam, which is offset from the incident beam by an angle

$$\theta' = 2 \sin^{-1} \left(\frac{\Lambda_o f_0}{2nv_a} \right) \tag{97}$$

inside the cell and an angle

$$\theta = 2 \sin^{-1} \left(\frac{\Lambda_o f_0}{2v_a} \right) \tag{98}$$

outside the cell. These equations are valid provided that the acoustic wave has a single wavelength across the cell. For small values of the argument, equation (98) becomes

$$\theta \simeq \frac{\Lambda_o f_0}{v_a} \quad , \quad \Lambda_o f_0 << 2v_a \quad . \tag{99}$$

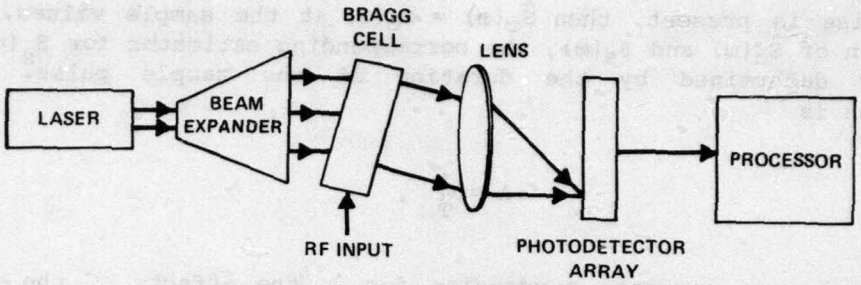

Figure 7. Acousto-optical spectrum analyzer.

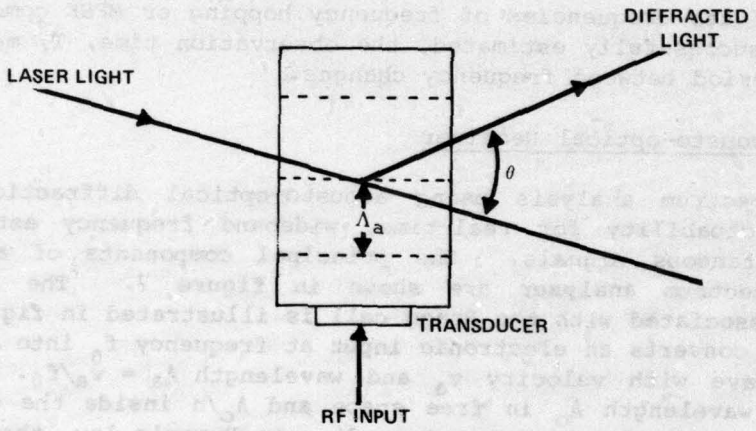

Figure 8. Acousto-optical diffraction geometry for input at single frequency.

The lens produces a Fourier transform on its focal plane at the photodetector array. The center of the diffracted beam converges to a position a distance

$$F\theta = \frac{F\Lambda_o f_0}{v_a} \tag{100}$$

from the center of the corresponding undiffracted beam, where F is the focal length of the transform lens. Thus, the frequency f_0 can be estimated by measuring the relative intensities at the photodetector array elements.[7]

[7] *D. L. Hecht, Spectrum Analysis Using Acousto-optic Filters, Optical Engineering, 16 (September 1977), 461.*

The diffracted beam has an angular width on the order of Λ_o/D, where D is the effective aperture of the Bragg cell. Consequently, the diffracted beam spreads over length of $F\Lambda_o/D$ in the focal plane. The frequency resolution is defined to be the difference in frequency between two intercepted signals such that the corresponding positions in the focal plane differ by the spread of the diffracted beam in the focal plane. From this definition and equation (100), the resolution is

$$\Delta \simeq \frac{v_a}{D} = \frac{1}{T_c} \quad , \tag{101}$$

where T_c is the time that it takes an acoustic wave to cross the cell aperture. This equation applies when an acoustic wave of fixed wavelength occupies the aperture. A necessary condition for its validity most of the time is that T_c be less than the period between frequency changes of a frequency-hopping signal or an MFSK signal. Thus, the resolution is no better than the inverse of the hopping period.

In frequency estimation, only one spatial dimension of the Bragg cell is used. It is possible to design a two-dimensional Bragg cell array to estimate frequency and direction of arrival simultaneously,[8] as shown in the schematic diagram of figure 9. The cell inputs are the outputs of spatially separated antennas. The intensity distribution across the photodetector array has one or more maxima that are vertically deflected proportionally to the intercepted signal frequencies and are horizontally deflected proportionally to the signal's angle of arrival. If the largest of the outputs of the photodetector elements is compared with a threshold, the presence of an intercepted signal can be determined. Thus, in principle, an acousto-optical system can detect hostile communications, estimate their frequencies, and find their directions.

3.4 Instantaneous Frequency Measurement

The instantaneous frequency measurement (IFM) receiver, illustrated in figure 10, is often used to estimate radar frequencies. It is possible to use it as a supplementary frequency estimator for communications, but usually not by itself. Its operation is based on the relationship among carrier frequency, path length, and phase shift of a signal. Suppose that, after passage through the bandpass filter of bandwidth W, an intercepted signal has the form

$$s(t) = A(t) \cos \left[\omega_0 t + \phi(t)\right] \quad , \tag{102}$$

---

[8] *R. A. Coppock, R. F. Croce, W. L. Regier, Bragg Cell RF Signal Processing, Microwave J. (September 1978), 62.*

where A(t) is the amplitude modulation and $\phi(t)$ is the angle modulation function. As shown in figure 10, this signal is delayed by time δ in one branch relative to the other branch. If δ is sufficiently small, then $A(t - \delta) \simeq A(t)$ and $\phi(t - \delta) \simeq \phi(t)$ for most of the time. It follows that

$$s_1(t) \simeq A(t) \cos \left[\omega_0 t + \phi(t) - \omega_0 \delta\right] , \tag{103}$$

$$A(t - \delta) \simeq A(t) \quad , \quad \phi(t - \delta) \simeq \phi(t).$$

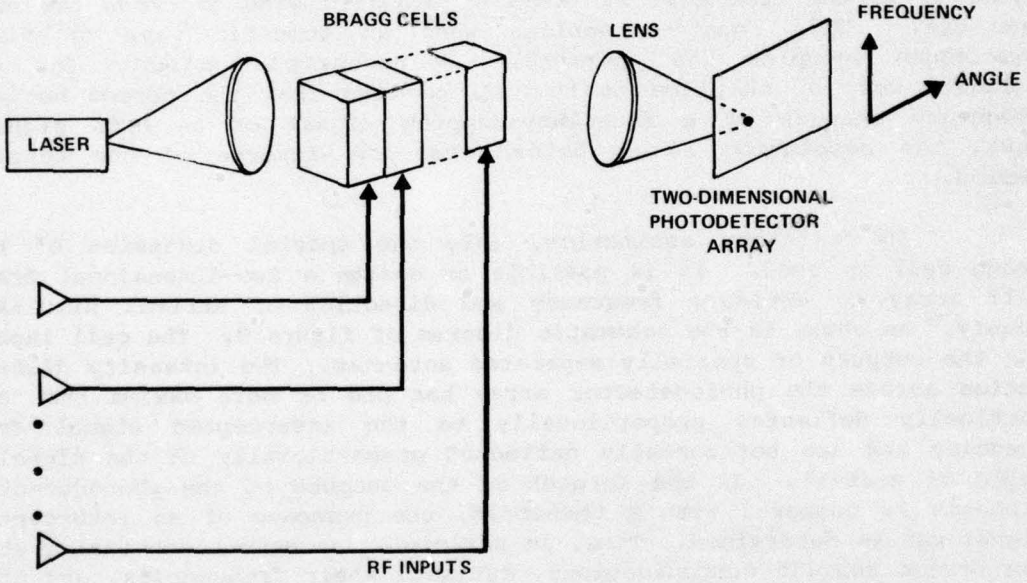

Figure 9. Array of Bragg cells for simultaneous frequency estimation and direction finding.

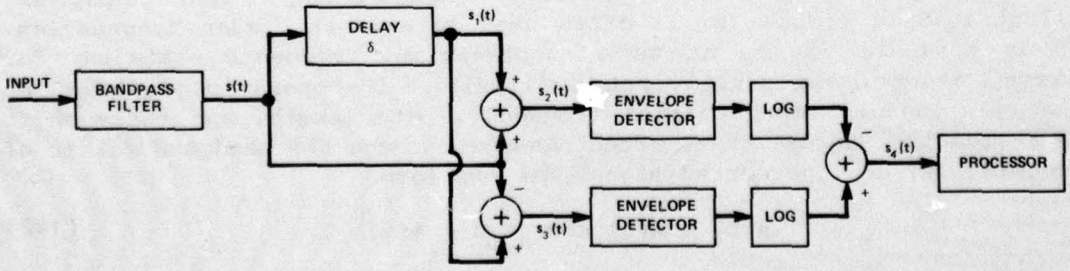

Figure 10. Instantaneous frequency measurement receiver.

By trigonometric identities, the outputs of the sum and difference operations in the figure are found to be

$$s_2(t) = \left[2A(t)\ \cos\left(\frac{\omega_0\delta}{2}\right)\right]\cos\left[\omega_0 t + \phi(t) - \frac{\omega_0\delta}{2}\right] , \qquad (104)$$

$$s_3(t) = \left[2A(t)\ \sin\left(\frac{\omega_0\delta}{2}\right)\right]\sin\left[\omega_0 t + \phi(t) - \frac{\omega_0\delta}{2}\right] \qquad (105)$$

for most of the time. The envelope detectors produce the magnitudes of the first factors in equations (104) and (105). These signals pass through logarithmic amplifiers, and the difference is taken. Thus, if $\omega_0\delta < \pi$, the processor input is proportional to

$$s_4(t) = \log \tan \omega_0\delta \ . \qquad (106)$$

Since the modulation effects have been removed and δ is known, the processor can calculate an estimate of $f_0 = \omega_0/2\pi$. The tangent function has an unambiguous inverse only over a range of π radians. Thus, for unambiguous operation over the frequency range of W hertz, we must have $\delta \leq 1/2W$. A major problem with the IFM receiver is that the resolution is inversely proportional to δ. Since δ must be sufficiently small so that equation (103) is valid for most of the time, the resolution may be inadequate. Another problem is that the IFM receiver cannot handle two or more simultaneously intercepted signals of comparable magnitudes.

3.5 Scanning Superheterodyne Receiver

Figure 11 shows a block diagram of a realization of a scanning superheterodyne receiver for frequency estimation. To explain the operation, we consider the system response to one scan of the local oscillator and an input that has constant amplitude, frequency, and phase over the scan period, T. The input is represented by

$$s(t) = A\cos\left(\omega_0 t + \theta\right) , \ 0 \leq t \leq T , \qquad (107)$$

where ω_0 is the carrier frequency and θ is the phase angle at $t = 0$, which defines the beginning of the scan. The scanning waveform, which is the output of a swept local oscillator, is proportional to

$$y(t) = \cos\left(\omega_s t - \pi\mu t^2\right) , \ 0 \leq t \leq T , \qquad (108)$$

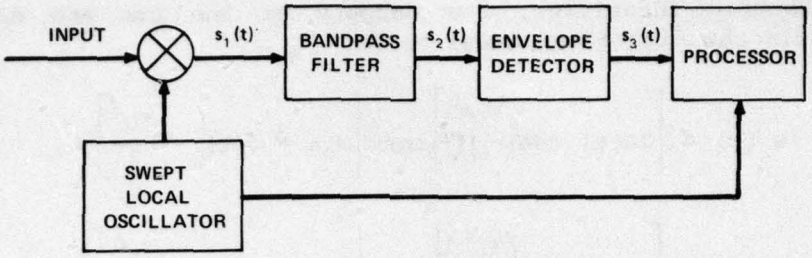

Figure 11. Scanning superheterodyne receiver.

where ω_s is the frequency at $t = 0$ and μ is the scan rate, which is the rate of frequency change. The output of the mixer, $s_1(t) = s(t)y(t)$, passes through a bandpass filter with impulse response $h(t)$ and bandwidth $2B$. Ignoring a high-frequency term that is suppressed by the bandpass filter, we have

$$s_1(t) = \frac{1}{2} A \cos\left(\omega_1 t + \pi\mu t^2 + \theta\right), \quad 0 \leq t \leq T, \tag{109}$$

where $\omega_1 = \omega_0 - \omega_s$.

The symmetrical bandpass filter has transfer function $H(\omega)$ that can be written as

$$H(\omega) = H_1\left(\omega - \omega_c\right) + H_1\left(\omega + \omega_c\right), \tag{110}$$

where $H_1(\omega)$ is the transfer function of a lowpass filter and ω_c is the center frequency of the bandpass filter. The first term on the right side has significant values only for positive frequencies, while the second term has significant values only for negative frequencies. If $h_1(t)$ is the impulse response of the lowpass filter, then

$$h(t) = 2h_1(t) \cos \omega_c t . \tag{111}$$

The output of the bandpass filter is

$$s_2(t) = \int_{-\infty}^{\infty} s_1(\tau) h(t - \tau)\, d\tau . \tag{112}$$

By using equations (109) and (111) and the pertinent trigonometric relations, equation (112) becomes

$$s_2(t) = \frac{A}{2} \int_0^T h_1(t - \tau) \cos \left[\left(\omega_1 - \omega_c \right) \tau + \pi\mu\tau^2 + \theta + \omega_c t \right] d\tau \tag{113}$$

$$+ \frac{A}{2} \int_0^T h_1(t - \tau) \cos \left[\left(\omega_1 + \omega_c \right) \tau + \pi\mu\tau^2 + \theta - \omega_c t \right] d\tau \ .$$

It is assumed that $H_1(\omega)$ has a sufficiently narrow bandwidth that the second integral on the right side of this equation is negligible. The time-frequency diagram of figure 12, in which $f = \omega/2\pi$, illustrates the effect of the filter. The filter output, $s_2(t)$, is significant only over a portion of the scan period. Thus, we can extend the limits of the first integral to $\pm\infty$ with negligible error if $f_1 + \mu T > f_c + B/2$ and $f_1 < f_c - B/2$. Under these assumptions,

$$s_2(t) = \frac{A}{2} \int_{-\infty}^{\infty} h_1(t - \tau) \cos \left(\omega_2 \tau + \pi\mu\tau^2 + \theta_1 \right) d\tau \ , \tag{114}$$

where $\omega_2 = \omega_0 - \omega_s - \omega_c$ and $\theta_1 = \theta + \omega_c t$. To further simplify equation (114), we assume a Gaussian bandpass filter; that is,

$$H_1(\omega) = \exp \left(- \frac{\omega^2}{4a^2} - j\omega\delta \right) \ , \tag{115}$$

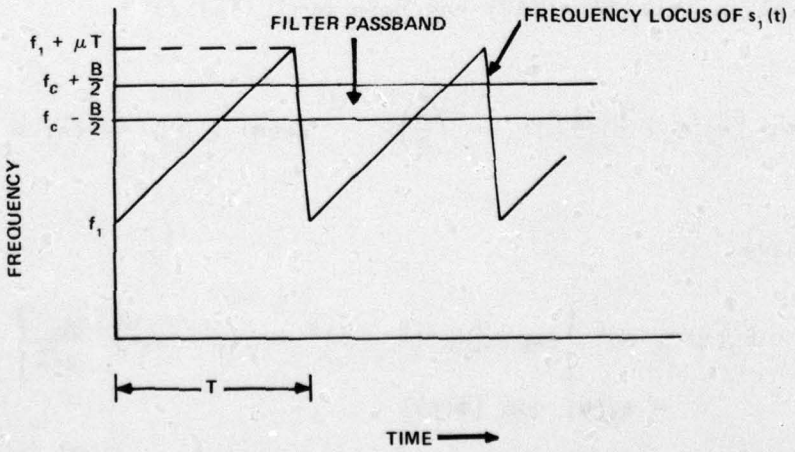

Figure 12. Time-frequency diagram for scanning superheterodyne receiver.

where parameter a is proportional to the bandwidth and δ is the filter delay. If δ is sufficiently large, equation (115) approximates a realizable filter. The corresponding impulse response is

$$h_1(t) = \frac{1}{2\pi} \int_{-\infty}^{\infty} H_1(\omega) e^{i\omega t}\, d\omega = \frac{a}{\sqrt{\pi}} \exp\left[-a^2(t-\delta)^2\right] . \quad (116)$$

Substituting equation (116) into equation (114), expressing the cosine in terms of complex exponentials, and simplifying the result, we obtain

$$s_2(t) = \mathrm{Re}\left\{\frac{Aa}{2\sqrt{\pi}} \exp\left[-a^2(t-\delta)^2 + j\theta_1 + sc^2\right] \times \int_{-\infty}^{\infty} \exp\left[-s(\tau + c)^2\right] d\tau\right\} , \quad (117)$$

where Re(x) denotes the real part of x and

$$s = a^2 - j\pi\mu ,$$
$$c = \frac{-2a^2(t-\delta) - j\omega_2}{2s} . \quad (118)$$

The integral in equation (117) has been evaluated as[5]

$$\int_{-\infty}^{\infty} \exp\left[-s(\tau + c)^2\right] d\tau = \left(\frac{\pi}{s}\right)^{1/2} , \ \mathrm{Re}(s) \geq 0 , \ \mathrm{Re}(\sqrt{s}) > 0 . \quad (119)$$

Thus, we have

$$s_2(t) = \mathrm{Re}\left\{\exp\left[-a^2(t-\delta)^2 + j\theta_1 + sc^2\right] \frac{Aa}{2\sqrt{s}}\right\} = s_3(t) \cos\left[\phi(t)\right] , \quad (120)$$

---

[5] *A. Papoulis, Signal Analysis, McGraw-Hill Book Co., New York (1977).*

where

$$\phi(t) = \frac{4\pi a^4 \mu (t - \delta)^2 + 4a^4 \omega_2 (t - \delta) - \pi \mu \omega_2^2}{4(a^4 + \pi^2 \mu^2)} + \theta_1 + \frac{1}{2} \tan^{-1} \left(\frac{\pi \mu}{a^2} \right)$$

$$s_3(t) = \frac{A}{2} \left(1 + \frac{\pi^2 \mu^2}{a^4} \right)^{-1/4} \exp \left[- \frac{a^2 \left(2\pi\mu t - 2\pi\mu\delta + \omega_2 \right)^2}{4\left(a^4 + \pi^2 \mu^2 \right)} \right] . \qquad (121)$$

As indicated in figure 11, $s_2(t)$ is applied to an envelope detector that extracts the envelope, $s_3(t)$, from the input. The peak value of $s_3(t)$ is attained when $t = \delta - (\omega_2/2\pi\mu) = \delta - (f_0 - f_s - f_c)/\mu$. Thus, the input frequency f_0 can easily be estimated from the time location of the peak value. The normalized peak value, α, which is defined as the peak value relative to A/2, the peak value for small μ, is

$$\alpha = \left(1 + \frac{\pi^2 \mu^2}{a^4} \right)^{-1/4} . \qquad (122)$$

The half-power points of $s_3(t)$ are determined by setting the exponential factor in equation (121) equal to $1/\sqrt{2}$. The pulse duration of $s_3(t)$ between half-power points is determined to be

$$T_p = \frac{a(2 \ln 2)^{1/2}}{\pi \mu} \left(1 + \frac{\pi^2 \mu^2}{a^4} \right)^{1/2} . \qquad (123)$$

The frequency resolution in hertz, Δ, as determined by the processor of figure 11, is approximately equal to μT_p, the frequency range scanned during pulse duration T_p. Thus, the resolution is

$$\Delta = \frac{a(2 \ln 2)^{1/2}}{\pi} \left(1 + \frac{\pi^2 \mu^2}{a^4} \right)^{1/2} . \qquad (124)$$

From equation (115), the 3-dB power spectrum bandwidth in hertz is related to parameter a by

$$B = \frac{(2 \ln 2)^{1/2}}{\pi} a . \qquad (125)$$

In terms of B, we can write

$$\alpha = \left(1 + 0.195 \frac{\mu^2}{B^4}\right)^{-1/4} , \tag{126}$$

$$\Delta = B \left(1 + 0.195 \frac{\mu^2}{B^4}\right)^{1/2} . \tag{127}$$

These equations were originally derived for the theory of spectrum analyzers.[9]

If the scan rate, μ, is high,

$$\alpha \simeq 1.5 \frac{B}{\sqrt{\mu}} , \quad \Delta \simeq 0.44 \frac{\mu}{B} , \quad \mu >> B^2 , \tag{128}$$

which clearly show the effects of increasing μ.

Using elementary calculus, we determine the optimal filter bandwidth, B_0, to minimize Δ. Substituting this value of B_0 into equation (127), we obtain Δ_0, the minimum resolution as a function of μ. The results are

$$B_0 = 0.664\sqrt{\mu} , \quad \Delta_0 = \sqrt{2}\, B_0 . \tag{129}$$

The corresponding normalized peak value is

$$\alpha_0 = 0.84 , \tag{130}$$

which is no longer a function of μ. If the optimal bandwidth is used, these equations indicate that the achievable resolution becomes worse as μ increases, but the peak value does not change.

---

[9] *M. Engelson and F. Telewski, Spectrum Analyzer Theory and Applications, Artech House, Inc., Dedham, MA (1974).*

3.6 Microscan Receiver

Improved resolution at a high scan rate can be achieved by a microscan receiver, which uses the compression of pulses. The microscan receiver (fig. 13a) includes a dispersive filter, whereas the scanning superheterodyne receiver includes a bandpass filter.

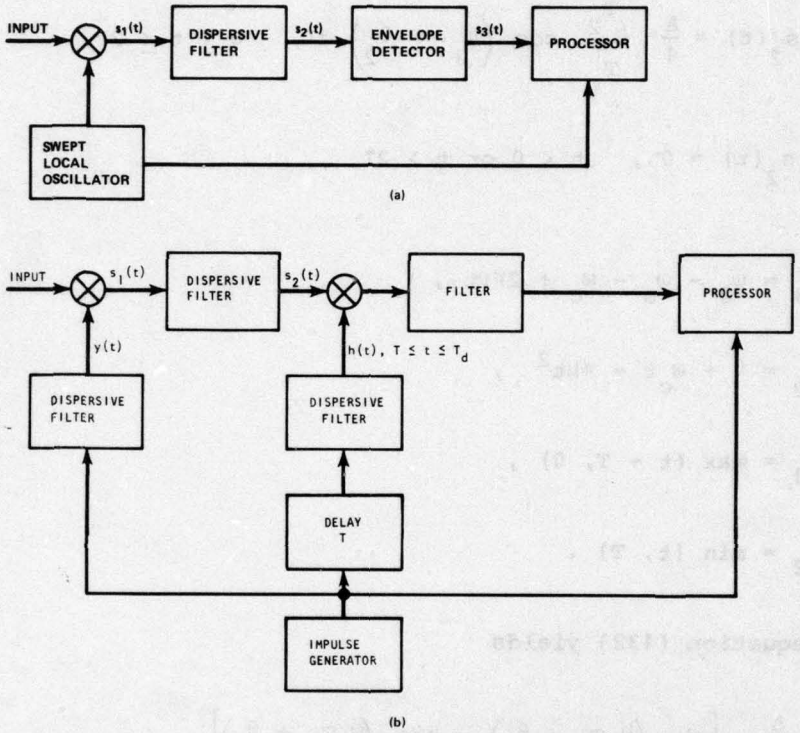

Figure 13. Microscan receivers for (a) frequency estimation or magnitude of Fourier transform and (b) real part of Fourier transform.

The impulse response of the dispersive filter is modeled as

$$h(t) = \cos\left(\omega_c t - \pi\mu t^2\right), \quad 0 \le t \le T_d, \tag{131}$$

where T_d is the duration of the impulse response and the amplitude has been normalized to unity. The dispersive filter can be realized by a surface acoustic wave device.[10] Substituting this equation and equation (109) into equation (112) yields the dispersive filter response to one

[10] *A. A. Oliner, ed., Acoustic Surface Waves, Springer-Verlag New York, Inc., New York (1978).*

scan of the local oscillator and an input represented by equation (107) over the scan period. Initially, we set $T_d = T$. Using $2 \cos u \cos v = \cos (u - v) + \cos (u + v)$, we may write the result as the sum of the two integrals. We assume that $|\omega_0 - \omega_s - \omega_c| \ll |\omega_0 - \omega_s + \omega_c|$ so that, for most values of t, we may neglect one of the integrals. We are left with the approximation

$$s_2(t) = \frac{A}{4} \int_{T_1}^{T_2} \cos \left(\omega_3 \tau + \theta_2 \right) d\tau, \quad 0 \leq t \leq 2T ,$$

$$s_2(t) = 0 , \quad t < 0 \text{ or } t > 2T , \tag{132}$$

where

$$\omega_3 = \omega_0 - \omega_s - \omega_c + 2\pi\mu t ,$$

$$\theta_2 = \theta + \omega_c t - \pi\mu t^2 , \tag{133}$$

$$T_1 = \max (t - T, 0) ,$$

$$T_2 = \min (t, T) .$$

If $\omega_3 \neq 0$, equation (132) yields

$$s_2(t) = \frac{A}{4\omega_3} \left[\sin \left(\omega_3 T_2 + \theta_2 \right) - \sin \left(\omega_3 T_1 + \theta_2 \right) \right] \tag{134}$$

$$= \frac{A}{2\omega_3} \sin \left[\frac{\omega_3}{2} \left(T_2 - T_1 \right) \right] \cos \left[\frac{\omega_3}{2} \left(T_1 + T_2 \right) + \theta_2 \right] .$$

The final form of equation (134) is valid even if $\omega_3 = 0$. For practical values of the parameters, the cosine factor varies much more rapidly with time than other factors. Consequently, using equations (133), the output of the envelope detector is

$$s_3(t) = \frac{At}{4} \operatorname{sinc} \left[\left(f_0 - f_s - f_c \right) t + \mu t^2 \right] , \quad 0 \leq t \leq T ,$$

$$s_3(t) = \frac{A(2T - t)}{4} \operatorname{sinc} \left[\left(f_0 - f_s - f_c + \mu t \right) \left(2T - t \right) \right] , \quad T \leq t \leq 2T , \tag{135}$$

where we have set $\omega = 2\pi f$.

The peak value of $s_3(t)$ is AT/4. We define parameter ε as

$$\varepsilon = f_s + f_c - f_0 - \mu T \ . \tag{136}$$

If the frequency of the intercepted signal is such that $\varepsilon = 0$, then the peak value of $s_3(t)$ occurs at $t = T$; that is,

$$s_3(T) = \frac{AT}{4} \ , \quad \varepsilon = 0 \ . \tag{137}$$

We also have

$$\begin{aligned} s_3\left(T \pm \frac{1}{2\mu T}\right) &\simeq \frac{AT}{4}\,(0.64) \ , \ \varepsilon = 0 \ , \ T \gg \frac{1}{\mu T} \ , \\ s_3\left(T \pm \frac{1}{\mu T}\right) &\simeq 0 \ , \quad \varepsilon = 0 \ , \quad T \gg \frac{1}{\mu T} \ . \end{aligned} \tag{138}$$

These equations indicate that $1/\mu T$ is an approximate measure of the width of the compressed output pulse. Satisfying the inequality ensures that the response of the microscan receiver due to one scan does not interact significantly with the response due to the next scan.

If the frequency of the intercepted signal shifts slightly, then $\varepsilon \neq 0$. A small shift yields

$$s_3\left(T + \frac{\varepsilon}{\mu}\right) \simeq \frac{AT}{4} \ , \ \left|\frac{\varepsilon}{\mu}\right| \ll T \ , \tag{139}$$

where the right side of the equation is the peak value of $s_3(t)$. Thus, the peak value occurs at time $t = T + \varepsilon/\mu$. Using equation (136), we can estimate the input frequency, $f_0 = \omega_0/2\pi$, from the time location of the peak value.

We define the resolution of the microscan receiver, Δ, as the value of the frequency shift in hertz, ε, that produces a shift in the time of the peak output equal to the width of the output when $\varepsilon = 0$. Thus,

$$\Delta = \frac{1}{T} = \frac{\mu}{W} \ . \tag{140}$$

where $W = \mu T$ is the total bandwidth scanned.

The ratio of the input pulse width to the compressed output pulse width is TW, which is called the compression ratio of the microscan receiver. When this ratio is large, a comparison of equations (140) and (129) indicates that there is a substantial improvement in resolution of the microscan receiver over the scanning superheterodyne receiver. A comparison of the receiver outputs for typical inputs of the form of equation (107) is depicted in figure 14.

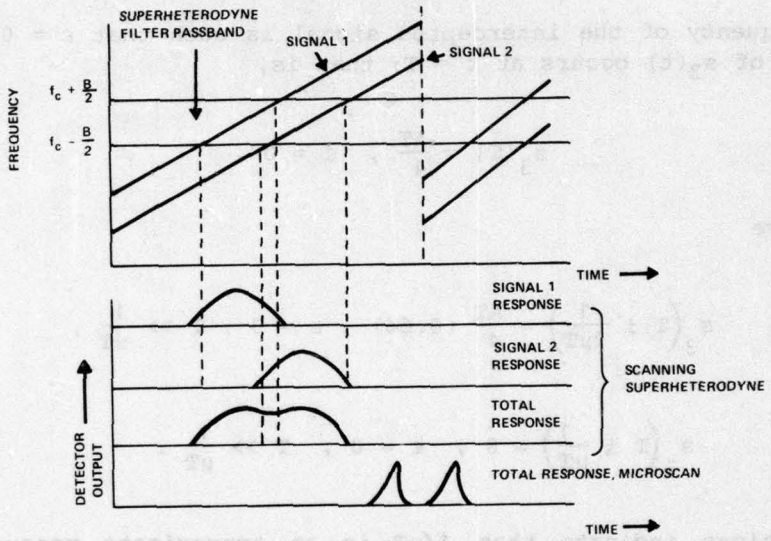

Figure 14. Response of scanning superheterodyne and microscan receivers to simultaneous signals.

Due to the presence of the sinc function, equation (135) exhibits smaller subsidiary peaks in addition to the main peak. In a multiple-target environment, these side lobes can mask adjacent main peaks due to other targets, thus limiting the frequency resolution and dynamic range of the receiver. Consequently, it is sometimes desirable to follow the dispersive filter with a shaping filter for side-lobe reduction or to modify the impulse response of the dispersive filter itself.

For a large compression ratio, the transfer function associated with equation (131) has a flat, nearly rectangular amplitude response and a quadratic phase response[11] over bandwidth W.

The preceding analysis is valid if the modulation period of the input is large compared with the scan period. If a more rapidly modulated input is present, the microscan receiver can be designed to

[11] *H. J. Blinchikoff and A. I. Zverev, Filtering in the Time and Frequency Domains, John Wiley and Sons, Inc., New York (1976).*

produce an output that is an approximation of the Fourier transform of the modulation. In this case, the system is often called a chirp transform processor. As previously, we consider the system response to one scan of the local oscillator. Over the scan period, the input is assumed to have the form

$$s(t) = s_0(t) \cos\left(\omega_0 t + \theta\right) , \quad 0 \leq t \leq T . \tag{141}$$

This input is mixed with the scanning waveform of equation (108) to produce

$$s_1(t) = \frac{1}{2} s_0(t) \cos\left(\omega_1 t + \pi\mu t^2 + \theta\right) , \quad 0 \leq t \leq T . \tag{142}$$

The impulse response of the dispersive filter is given by equation (131), where we assume that $T_d \geq T$. We calculate the system output in the time interval $T \leq t \leq T_d$. Substituting equations (142) and (131) into equation (112), using trigonometry, dropping a negligible integral, and substituting a complex exponential, we obtain

$$s_2(t) = \mathrm{Re}\left\{\frac{1}{4} \exp\left[j\left(\omega_c t - \pi\mu t^2 + \theta\right)\right] \int_{-\infty}^{\infty} s_0(\tau) q(\tau) \exp\left[-j\tau\left(\omega_c - \omega_1 - 2\pi\mu t\right)\right] d\tau\right\}$$

$$= \mathrm{Re}\left\{\frac{1}{4} \exp\left[j\left(\omega_c t - \pi\mu t^2 + \theta\right)\right] S_0\left(\omega_c - \omega_1 - 2\pi\mu t\right)\right\}$$

$$= \frac{1}{4} \left|S_0\left(\omega_c - \omega_1 - 2\pi\mu t\right)\right| \cos\left[\omega_c t - \pi\mu t^2 + \theta + \phi\left(\omega_c - \omega_1 - 2\pi\mu t\right)\right] ,$$

$$T \leq t \leq T_d , \tag{143}$$

where $q(t)$ is defined in equation (85), $S_0(\omega)$ is the Fourier transform of $s_0(\tau)q(\tau)$, and $\phi(\omega)$ is the phase angle of the Fourier transform. The output of the envelope detector is proportional to

$$s_3(t) = \left|S_0\left(\omega_s + \omega_c - \omega_0 - 2\pi\mu t\right)\right| , \quad T \leq t \leq T_d . \tag{144}$$

Thus, the magnitude of the Fourier transform of the input modulation has been produced as a time signal.

If $s_2(t)$ is multiplied by $h(t)$, then equations (131) and (143) indicate that, after elimination of a double frequency term by filtering, the phase-shifted real part of $S_0(\omega)$ is produced as a time signal. As shown in figure 13(b) the waveform $h(t)$, $T \leq t \leq T_d$, can be produced by applying an impulse at time T to a dispersive filter with impulse response $h_1(t) = h(t + T)$, $0 \leq t \leq T_d - T$. The phase-shifted imaginary part of $S_0(\omega)$ can be produced as a time signal by multiplying $s_2(t)$ by $\sin(\omega_c t - \pi\mu t^2)$.

Let ω_m denote the maximum value of ω for which $|S_0(\omega)|$ has a significant value. If

$$T + \frac{\omega_m}{2\pi\mu} \leq \frac{\omega_s + \omega_c - \omega_0}{2\pi\mu} \leq T_d , \tag{145}$$

then during the time interval $T \leq t \leq T_d$, $s_3(t)$ exhibits all the values of $|S_0(\omega)|$ for $0 \leq \omega \leq \omega_m$. The range of possible values of $f_0 = \omega_0/2\pi$ for which equation (145) can be satisfied is

$$W_R = \mu T_d - f_m - \mu T , \quad T_d \geq T + \frac{f_m}{\mu} , \tag{146}$$

where $f_m = \omega_m/2\pi$. If we wish to avoid the interference of the Fourier transform generated by a scan, which occurs during $T \leq t \leq T_d$, with the Fourier transform generated by the next scan, then we set $T_d \leq 2T$. In terms of the total bandwidth scanned, $W = \mu T$, we have

$$0 \leq W_R \leq W\left(1 - \frac{f_m}{W}\right), \quad T + \frac{f_m}{\mu} \leq T_d \leq 2T . \tag{147}$$

If $f_m << W$ and $T_d = 2T$, then $W_R \simeq W$.

The inequality for T_d in equation (147) is necessary for satisfactory spectral analysis. However, for frequency estimation alone, setting $T_d = T$ not only is adequate, but also minimizes the interference between scan responses.

The chirp transform processor can be used as the basic building block of an analog version of the cross correlator of figure 5.

In addition to frequency estimation, the microscan receiver can be used for detection. Alternatively, if interception is verified by a parallel system designed expressly for that purpose, frequency can be estimated by the microscan receiver.

If the scanning period is less than the period between frequency changes of the intercepted signal, the microscan and scanning superheterodyne receivers can estimate each frequency of a frequency-hopping or MFSK signal. If not, some frequencies may be missed, and the estimation accuracy is degraded. The inherent linearity of these two receivers makes them potentially effective in analyzing many simultaneous intercepted signals.

4. DIRECTION FINDING

Signals must be detected, and sometimes the frequency must be estimated, if direction is to be found. Conversely, direction finding provides signal sorting, which restricts the number of signals that the detection and frequency estimation systems must process simultaneously.

For simplicity, the estimation of a single bearing angle is considered. In a ground-based interception system, an azimuth angle may be all that is needed. However, airborne systems may require estimates of both the azimuth and the elevation angles to the intercepted transmitter.

4.1 Energy Comparison Systems

Energy comparison systems are analogous to the amplitude comparison systems used in radar[12], but when communications with unknown parameters are to be intercepted, it is logical to base comparisons upon the energy rather than the amplitude. The stationary multibeam system for direction finding is illustrated in figure 15. First, the largest of the receiver outputs is selected. Next, the larger of the two receiver outputs corresponding to beams adjacent to the beam that produced the largest output is selected. The two selected outputs are denoted by L_1 and L_2. The processor compares the outputs to a threshold for detection. The angle of arrival is estimated from the logarithm of the ratio of L_1 to L_2. The radiation patterns of the adjacent beams are illustrated in figure 16, where ϕ represents the angle of arrival of an intercepted signal, and beam pattern $F_i(\theta)$ produces L_i. The origin of the coordinate system is defined so that $+\psi$ and $-\psi$ indicate the peak responses of the two beams, respectively. Suppose that the beam patterns are approximately Gaussian; that is, they are described by

$$F_1(\theta) = K_1 \exp\left[-\frac{(\theta - \psi)^2}{b^2}\right] , \qquad (148)$$

---

[12] *D. K. Barton, Radar System Analysis, Artech House, Inc., Dedham, MA (1976).*

$$F_2(\theta) = K_2 \exp\left[-\frac{(\theta + \psi)^2}{b^2}\right], \tag{149}$$

where K_1 and K_2 are constants independent of θ, and b is a measure of the beam width. If the receivers contain radiometers, then the L_i are proportional to the squares of the F_i. Thus, in the absence of noise, the processor input is

$$Z = \ln \frac{L_1(\phi)}{L_2(\phi)} = 2 \ln \frac{K_1}{K_2} + \frac{8\psi\phi}{b^2}. \tag{150}$$

The angle of arrival can be determined by inverting this equation. In the presence of noise, the same inverse provides an estimate, $\hat{\phi}$, of the actual angle ϕ. We have

$$\hat{\phi} = \frac{b^2}{8\psi}\left(Z - 2 \ln \frac{K_1}{K_2}\right), \tag{151}$$

where Z is now a random variable. Since $\hat{\phi}$ is a linear function of Z, the required processing is quite simple. We give an error analysis assuming that L_1 and L_2 are correctly chosen.

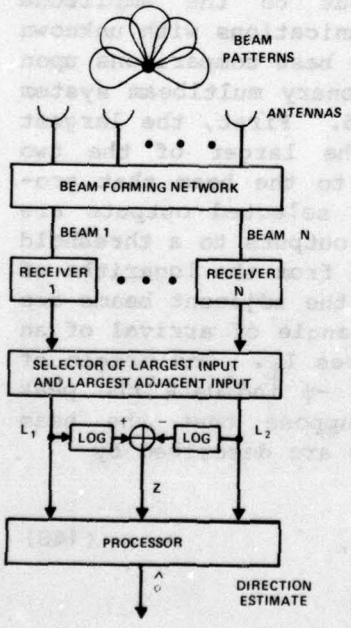

Figure 15. Stationary multibeam system.

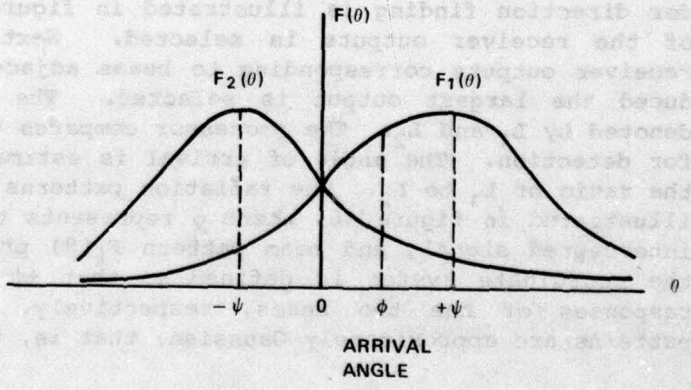

Figure 16. Adjacent antenna radiation patterns.

Because L_1 and L_2 are the outputs of radiometers, they are statistically independent, noncentral χ^2 random variables with γ degrees of freedom and noncentral parameters λ_1 and λ_2, respectively. From elementary probability theory, the probability density function of $Y = L_1/L_2$, the quotient of two nonnegative random variables, is

$$p_2(y) = \int_0^\infty x p_{11}(yx) p_{12}(x)\, dx , \quad y \geq 0 ,$$
$$p_2(y) = 0 , \quad y < 0 , \tag{152}$$

where $p_{11}(x)$ and $p_{12}(x)$ are the density functions for L_1 and L_2, respectively. The density function $p_{1i}(x)$ is given by equation (30) with λ_i substituted for λ. The noncentral parameters are given by

$$\lambda_1 = \frac{2E_1}{N_0} \exp\left[-\frac{2(\phi - \psi)^2}{b^2}\right] ,$$
$$\lambda_2 = \frac{2E_2}{N_0} \exp\left[-\frac{2(\phi + \psi)^2}{b^2}\right] , \tag{153}$$

where E_i is the energy received when the intercepted signal enters the center of the beam associated with L_i.

From equations (151) to (153) and the fact that $Z = \ln Y$, we can determine the root-mean-square error of $\hat{\phi}$, which we denote by E_R. By definition and a straightforward expansion,

$$E_R^2 = E\left[(\hat{\phi} - \phi)^2\right] = VAR(\hat{\phi}) + B_\phi^2 , \tag{154}$$

where $VAR(\hat{\phi})$ is the variance of $\hat{\phi}$ and B_ϕ is the bias,

$$B_\phi = E\left[\hat{\phi}\right] - \phi . \tag{155}$$

To evaluate E_R, we need the first two moments of Z. For simplicity, we assume that $K_1 = K_2$ and $E_1 = E_2$. When $\phi = 0$, equations (153) give $\lambda_1 = \lambda_2$ so that L_1 and L_2 are identically distributed random variables.

Since $Z = \ln L_1 - \ln L_2$, it follows that

$$E[Z] = 0 \ , \quad \phi = 0 \ . \tag{156}$$

At other values of ϕ, closed-form expressions for the mean and other moments are difficult to obtain. In general, the distribution of L_1 at ϕ is identical to the distribution of L_2 at $-\phi$. Thus, E_R is symmetric about $\phi = 0$.

To obtain an approximate expression for E[Z], we write the integral for E[ln Y] as a double integral and change coordinates:

$$E[Z] = \int_0^\infty \int_0^\infty x \ln y \, p_{11}(yx) p_{12}(x) \, dx \, dy$$

$$= \int_0^\infty \int_0^\infty \ln\left(\frac{v}{x}\right) p_{11}(v) p_{12}(x) \, dx \, dv \ . \tag{157}$$

The logarithm is approximated by the first six terms of its two-dimensional Taylor series expansion about the point $v = m_1$, $x = m_2$, where m_1 and m_2 are the mean values of L_1 and L_2, respectively. Thus,

$$\ln\left(\frac{v}{x}\right) \simeq \ln\left(\frac{m_1}{m_2}\right) + \frac{v - m_1}{m_1} - \frac{x - m_2}{m_2} - \frac{(v - m_1)^2}{2m_1^2}$$

$$+ \frac{(x - m_2)^2}{2m_2^2} - \frac{(v - m_1)(x - m_2)}{2m_1 m_2} \ . \tag{158}$$

This approximation is accurate over some range of v and x about $v = m_1$, $x = m_2$. If $p_{11}(v)$ and $p_{12}(x)$ are negligible outside this range, then the substitution of equation (158) into equation (157) yields an accurate approximation of E[Z]. The ranges of significant values of $p_{11}(v)$ and $p_{12}(x)$ are approximately limited by $|v - m_1| < 3\sigma_1$ and $|x - m_2| < 3\sigma_2$, where σ_1 and σ_2 are the standard deviations of L_1 and L_2, respectively. Thus, sufficient conditions for the valid use of equation (158) are $\sigma_1 \ll m_1$ and $\sigma_2 \ll m_2$.

Making the substitution and using the properties of density functions, we obtain

$$E[Z] \simeq \ln\left(\frac{m_1}{m_2}\right) - \frac{\sigma_1^2}{2m_1^2} + \frac{\sigma_2^2}{2m_2^2} \quad , \quad \sigma_1 << m_1 \quad , \quad \sigma_2 << m_2 \quad . \tag{159}$$

From equations (26) and (27), we have

$$m_i = \lambda_i + 2\gamma \quad , \quad i = 1, 2 \quad , \tag{160}$$

$$\sigma_i^2 = 4\lambda_i + 4\gamma \quad , \quad i = 1, 2 \quad . \tag{161}$$

An approximate expression for $E[Z^2]$ is obtained in an analogous manner. Combining this expression with equation (159) and dropping terms higher than second order in σ_1/m_1 and σ_2/m_2, we obtain

$$VAR(Z) \simeq \frac{\sigma_1^2}{m_1^2} + \frac{\sigma_2^2}{m_2^2} \quad , \quad \sigma_1 << m_1 \quad , \quad \sigma_2 << m_2 \quad . \tag{162}$$

By using $K_1 = K_2$ and equations (151), (154), (159), and (162), an equation for E_R can be derived,

$$E_R = \frac{b^2}{8\psi}\left\{\frac{\sigma_1^2}{m_1^2} + \frac{\sigma_2^2}{m_2^2} + \left[\ln\left(\frac{m_1}{m_2}\right) - \frac{\sigma_1^2}{2m_1^2} + \frac{\sigma_2^2}{2m_2^2} - \frac{8\psi\phi}{b^2}\right]^2\right\}^{1/2} ,$$

$$\sigma_1 << m_1 \quad , \quad \sigma_2 << m_2 \quad . \tag{163}$$

Figures 17 and 18 show representative plots of E_R versus ϕ. Figure 17 illustrates the effect of the normalized beam width, b/ψ, on E_R. For $E/N_0 = 10^4$, $\gamma = 10^3$, and $\phi = \psi$ the normalized beam width that minimizes E_R is approximately 4.5. However, the curves show that this normalized beam width is not optimal for other values of ϕ. Figure 18 illustrates the effect of increasing the observation interval, T. Since an increase in T causes proportionate increases in E and γ, we set $E/N_0 = 10\gamma$ for each value of γ. The optimal normalized beam width for each value of γ and $\phi = \psi$ is chosen. The curves show a steady decrease in E_R as γ increases.

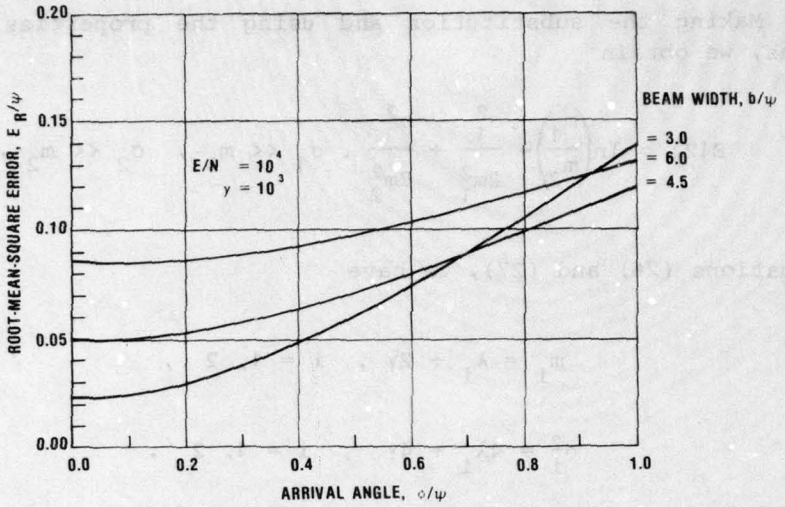

Figure 17. Root-mean-square error versus arrival angle for different beam widths.

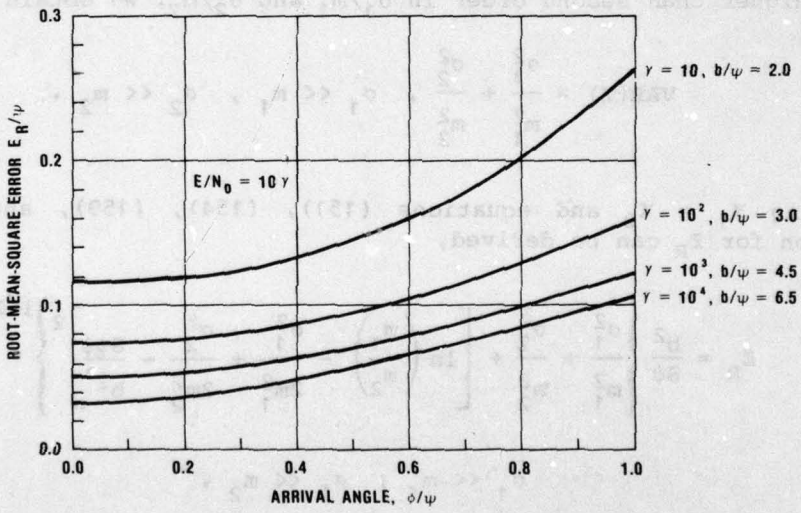

Figure 18. Root-mean-square error versus arrival angle for optimal beam widths and different values of γ.

Suppose many frequency-hopping signals are simultaneously intercepted by a channelized receiver. If it is impossible to correlate successive hopping frequencies, the direction of a signal must be estimated on the basis of the energy received in a single channel during a single hopping period. With this interpretation, γ is proportional to the hopping period, and figure 18 indicates the loss in directional accuracy resulting from an increase in hopping rate.

Energy comparison with a rotating beam is illustrated in figure 19. A rotating dish or an electronically scanned phased array is used with an omnidirectional antenna a small distance apart. The receivers are radiometers. Detection of a signal is verified and an estimate of direction is obtained by measuring the ratio of L_1 to L_2 and comparing the ratio to a threshold. Because a ratio is used, the effects of amplitude modulation and rotation can be largely eliminated by the processor. Signals entering through the side lobes and the back lobes of the rotating beam are inhibited. Alternatively, if two simultaneously rotating beams are offset relative to each other, sum and difference outputs can be produced (fig. 20), as in monopulse radar systems. If the intercepted signal duration is sufficient, the accuracy of the direction estimates of the systems of figures 19 and 20 can be improved by continued processing. After the target is detected, the rotation slows or stops. Processing over an increased observation interval allows further adjustment of antenna position until the intercepted signal's direction of arrival is fixed near the center of the rotating beam or beams.

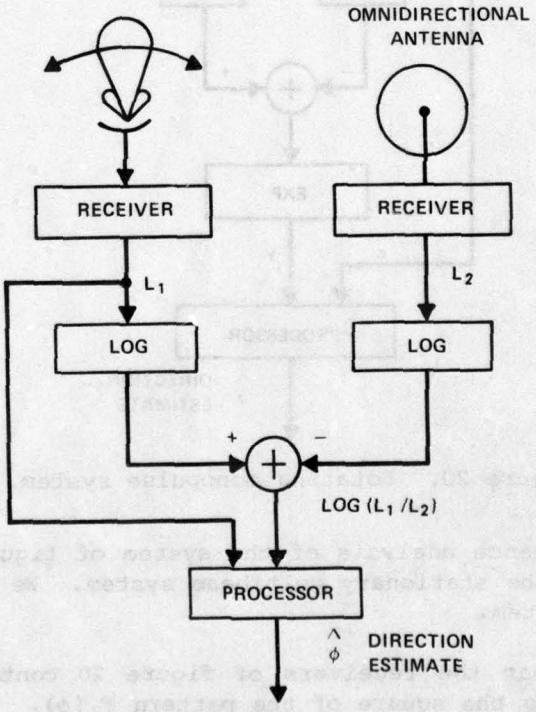

Figure 19. Rotating beam system.

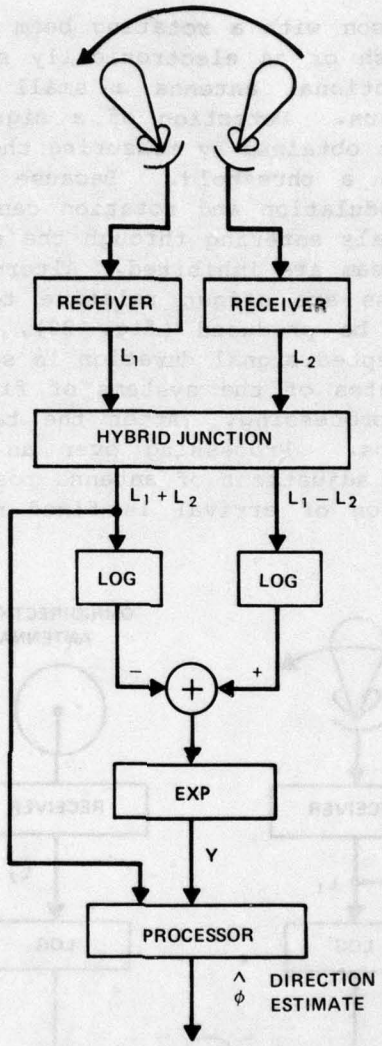

Figure 20. Rotating monopulse system.

The performance analysis of the system of figure 19 is similar to the analysis of the stationary multibeam system. We give an analysis of the monopulse system.

Assuming that the receivers of figure 20 contain radiometers, L_i is proportional to the square of the pattern $F_i(\phi)$. It follows that, in the absence of noise,

$$Y = \frac{L_1 - L_2}{L_1 + L_2} = \frac{F_1^2(\phi) - F_2^2(\phi)}{F_1^2(\phi) + F_2^2(\phi)} . \qquad (164)$$

If the antenna beam patterns are given by equations (148) and (149) with $K_1 = K_2$, then

$$Y = \tanh \frac{4\psi\phi}{b^2} . \tag{165}$$

The angle of arrival can be determined by inverting equation (165). In the presence of noise, the same inversion provides an estimate of the actual angle. Near $\phi = 0$, the estimate is approximated by

$$\hat{\phi} \simeq \frac{b^2}{4\psi} Y , \quad \phi << \frac{b^2}{4\psi} , \tag{166}$$

where Y is now a random variable.

The probability density function of Y is complicated. However, the first two moments of Y can be approximately determined without explicitly deriving the density. By definition,

$$E\left[Y^n\right] = \int_0^\infty \int_0^\infty \left(\frac{x - v}{x + v}\right)^n p_{11}(x) p_{12}(v)\, dx\, dv . \tag{167}$$

Proceeding in a manner analogous to the evaluation of equation (157), we derive equations for E[Y] and VAR(Y) from equation (167) with n = 1, 2. Using equations (154) and (166) and retaining only second order terms in σ_1/m_1 and σ_2/m_2, we obtain

$$E_R = \frac{b^2}{4\psi} \left\{ \frac{4\left(m_2^2\sigma_1^2 + m_1^2\sigma_2^2\right)}{\left(m_1 + m_2\right)^4} + \left[\frac{m_1 - m_2}{m_1 + m_2} - \frac{2\left(m_2\sigma_1^2 - m_1\sigma_2^2\right)}{\left(m_1 + m_2\right)^3} - \frac{4\psi\phi}{b^2} \right]^2 \right\}^{1/2} , \tag{168}$$

$$\phi << \frac{b^2}{4\psi} , \quad \sigma_1 << m_1 , \quad \sigma_2 << m_2 .$$

At $\phi = 0$, we have $m_1 = m_2 = m$ and $\sigma_1 = \sigma_2 = \sigma$ so that

$$E_R = \frac{\sqrt{2}b^2\sigma}{8\psi m} , \quad \phi = 0 , \quad \sigma << m . \tag{169}$$

Appropriate substitution into this equation indicates that we can achieve $E_R << b$ if the observation interval, T, is sufficiently large. Thus, the potential direction-finding accuracy is much better than a beam width.

To compare this result with the corresponding result for the stationary multibeam array, we set $m_1 = m_2 = m$, $\sigma_1 = \sigma_2 = \sigma$, and $\phi = 0$ in equation (163). The result is equation (169). Thus, if $\phi = 0$, the stationary multibeam array performs as well as the monopulse system. However, if $\phi \neq 0$, E_R increases in the multibeam case. In the monopulse case, if the intercepted signal duration is sufficient, the antennas can adjust their positions until $\phi \simeq 0$ so that the E_R after adjustment is given by equation (169). The main disadvantage with the monopulse or other rotating beam system is the narrow instantaneous field of view, which may cause a signal to be missed or may decrease the possible observation time. On the other hand, when many hostile communications are present, the narrow field of view provides a valuable signal-sorting capability.

4.2 Interferometer

Another direction-finding system is the interferometer, which also forms the heart of phase-comparison monopulse radar systems.[12] An interferometer consists of two or more antennas or groups of elements of a phased array that use phase or arrival-time information to estimate direction (fig. 21). The antennas may be rotating and directional.

We first consider the interferometer of figure 21(a). Suppose a plane wave arrives at angle ϕ, where $|\phi| \leq \pi/2$. If two antennas are separated by distance d, then since phase angles are modulo 2π numbers, the phase difference between the antenna outputs is

$$\theta = \frac{2\pi d \sin \phi}{\Lambda_s} - 2\pi n , \quad |\theta| \leq \pi , \quad |\phi| \leq \frac{\pi}{2} , \tag{170}$$

---

[12] *D. K. Barton, Radar System Analysis, Artech House, Inc., Dedham, MA (1976).*

where Λ_s is the signal wavelength and n is an integer that ensures satisfaction of the first inequality. If $d \leq \Lambda_s/2$, then $n = 0$. If $d > \Lambda_s/2$, then n varies with ϕ, taking negative and positive values and the value zero.

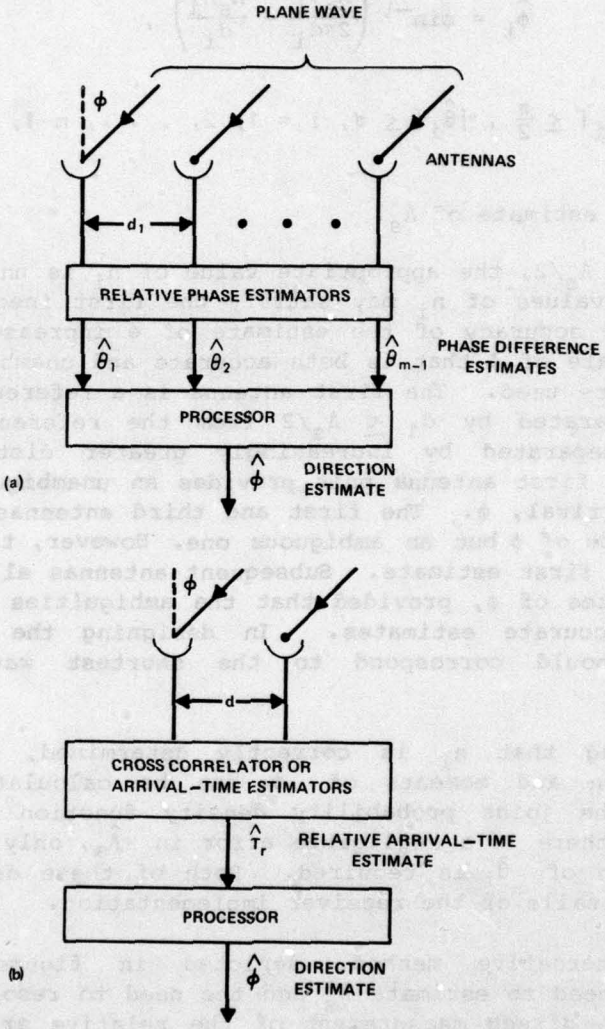

Figure 21. Interferometers using (a) phase information and (b) arrival-time information.

One antenna output provides a reference. Each of the other antenna outputs is applied to a separate device that estimates its phase relative to the reference. This device may be similar to the part of the IFM receiver in figure 10 that is fed by $s(t)$ and $s_1(t)$. The estimates of the relative phases are denoted by $\hat{\theta}_i$.

Estimates of the angle of arrival are calculated from the $\hat{\theta}_i$ by inverting equation (170). If there are m antennas, the (m - 1) estimates are given by

$$\hat{\phi}_i = \sin^{-1}\left(\frac{\hat{\Lambda}_s \hat{\theta}_i}{2\pi d_i} + \frac{\hat{\Lambda}_s n_i}{d_i}\right), \tag{171}$$

$$|\hat{\phi}_i| \leq \frac{\pi}{2}, \; |\hat{\theta}_i| \leq \pi, \; i = 1, 2, \ldots, m-1,$$

where $\hat{\Lambda}_s$ is an estimate of Λ_s.

Unless $d_i \leq \Lambda_s/2$, the appropriate value of n_i is unknown. In fact, many different values of n_i may satisfy the first inequality. On the other hand, the accuracy of the estimate of ϕ increases with d_i. To obtain an estimate of ϕ that is both accurate and unambiguous, three or more antennas are used. The first antenna is a reference. The second antenna is separated by $d_1 \leq \Lambda_s/2$ from the reference. The other antennas are separated by increasingly greater distances from the reference. The first antenna pair provides an unambiguous estimate of the angle of arrival, ϕ. The first and third antennas provide a more accurate estimate of ϕ but an ambiguous one. However, this ambiguity is resolved by the first estimate. Subsequent antennas allow increasingly accurate estimates of ϕ, provided that the ambiguities can be resolved by the less accurate estimates. In designing the interferometer, distance d_1 should correspond to the shortest wavelength to be intercepted.

Assuming that n_i is correctly determined, the probability density function and moments of $\hat{\phi}_i$ can be calculated by standard methods once the joint probability density function of $\hat{\theta}_i$ and $\hat{\Lambda}_s$ is specified. If there is a negligible error in $\hat{\Lambda}_s$, only the probability density function of $\hat{\theta}_i$ is required. Both of these density functions depend on the details of the receiver implementation.

An alternative method, depicted in figure 21(b), which eliminates the need to estimate Λ_s and the need to resolve ambiguities, is based on the direct measurement of the relative arrival time of a plane wave at two antennas. This relative arrival time can be estimated by using the vector output, D_i, of the cross correlator in figure 5, or by using two arrival-time estimators.

Assuming that a plane wave is received, the relative arrival time is given by

$$\tau_r = \frac{d \sin \phi}{v_e}, \; |\phi| < \frac{\pi}{2}, \tag{172}$$

where v_e is the speed of electromagnetic waves. Consequently, the angle of arrival estimator is

$$\hat{\phi} = \sin^{-1}\left(\frac{v_e \hat{T}_r}{d}\right) \quad , \quad |\hat{\phi}| < \frac{\pi}{2} \quad , \tag{173}$$

where $\hat{T}_r$ is the relative arrival-time estimator. Retaining the first three terms of a Taylor series expansion of equation (173) about the point T_r and using equation (172), we obtain

$$\hat{\phi} \simeq \phi + \frac{v_e}{d \cos \phi}\left(\hat{T}_r - T_r\right) + \frac{v_e^2 \sin \phi}{2d^2 \cos^3 \phi}\left(\hat{T}_r - T_r\right)^2 \quad , \quad |\phi| < \pi/2 \quad , \tag{174}$$

If $\hat{T}_r$ provides an unbiased estimate of T_r, then

$$E\left[\hat{T}_r\right] = T_r \quad . \tag{175}$$

It follows that

$$E\left[\hat{\phi}\right] = \phi + \frac{v_e^2 \sin \phi}{2d^2 \cos^3 \phi} \mathrm{VAR}\left(\hat{T}_r\right) \quad , \quad |\phi| < \pi/2 \quad . \tag{176}$$

Equation (176) shows that the angle estimator is biased even if the arrival-time estimator is unbiased. A straightforward calculation yields the variance of $\hat{\phi}$.

The root-mean-square error of $\hat{\phi}$ is obtained by substituting equation (174) into equation (154). By retaining only the lowest order term, the result is

$$E_R = \frac{v_e}{d \cos \phi} \sigma\left(\hat{T}_r\right) \quad , \quad |\phi| < \frac{\pi}{2} \quad , \tag{177}$$

where $\sigma(\hat{T}_r)$ is the standard deviation of $\hat{T}_r$. If $\phi = 0$, E_R has its minimal value. We have

$$E_R = \frac{V_e}{d}\,\sigma\left(\hat{T}_r\right) , \quad \phi = 0 . \tag{178}$$

This equation indicates that large antenna separations are sometimes necessary if E_R is to be small. For example, if $\sigma(\hat{T}_r) = 100$ ns and we desire $E_R = 0.05$ radians, then we need d = 600 m. However, unless the antenna separation is much smaller than the distance to the source of the intercepted signal, the plane wave assumption and, hence, equation (178) do not apply.

To determine $\mathrm{VAR}(\hat{T}_r)$, we must specify the details of the relative arrival-time estimation. For example, if the relative arrival time is computed by subtracting one arrival time from another and if the arrival times are statistically independent with equal variances, $\mathrm{VAR}(\hat{T}_r)$ is twice the variance of the arrival times. Expressions for the latter variance and various methods for arrival-time estimation can be found in the literature.[13,14]

5. CONCLUSIONS

When little is known about a signal to be intercepted, the signal energy and the autocorrelation function present two natural characteristics upon which the interception receiver can base its processing. A radiometer, which measures the signal energy, and a cross correlator, which estimates the autocorrelation function, perform similarly as detectors. The choice between using a radiometer and using a cross correlator is best made on the basis of the additional hardware needed for the receiver's other functions. For example, if a Fourier analysis of the signal and the direction finding with an interferometer are planned, then detection with a cross correlator is preferable since it requires little additional hardware.

A receiver is channelized if its total bandwidth is divided into M parts by a filter bank, and the filter outputs are processed in parallel. Against narrowband communications, the intercepted power required by a channelized receiver is reduced by a factor of $\sqrt{M}$ compared with a wideband receiver with the same total bandwidth. Channelized receivers often improve performance against frequency-hopping communications, although a sufficiently high hopping rate may render a channelized design impractical. Pseudonoise spread-spectrum communications require preliminary processing before being applied to a channelized receiver.

---

[13] *B. N. Mityashev, The Determination of the Time Position of Pulses in the Presence of Noise, MacDonald, London (1965).*

[14] *D. J. Torrieri, Adaptive Thresholding Systems, IEEE Trans. Aerosp. Electron. Syst., 13 (May 1977), 273.*

Channelized receivers, digital filters, acousto-optical devices, and microscan receivers (chirp transform processors) provide comparable resolutions as frequency estimation systems. The systems also theoretically can handle multiple signals that are simultaneously intercepted. The IFM and scanning superheterodyne receivers are less attractive systems in terms of potential capabilities, but may be useful as auxiliary frequency estimators. If speed of frequency estimation is important, it is desirable to use channelized receivers, microscan receivers, or acousto-optical devices with parallel readout of the photodetector outputs. All three systems can provide detection with little additional hardware. In choosing among these three systems, cost and practical implementation problems are among the most important considerations.

If widely separated antennas can be deployed and if the signal to be intercepted has a narrow autocorrelation function, then an interferometer is an effective system for direction finding. Under other circumstances, energy comparison systems and possibly acousto-optical devices are attractive alternatives. Energy comparison systems can be either stationary or rotating. Rotating systems can adjust the antenna position to increase the angle estimation accuracy. When many hostile communications are present, the narrow field of view provides a valuable signal-sorting capability. However, a narrow instantaneous field of view may cause a signal to be missed or may decrease the possible observation time, thereby decreasing the angle estimation accuracy.

By what electronic countermeasures can the communicators thwart interception? The data rates and the transmission powers can be kept to a minimum. Cables and optical fiber links are very helpful whenever feasible. Directional antennas help to conceal the existence of communications from the opponent. However, there are constraints on the degree of directionality that can be designed into an antenna to be used in the battlefield. An important constraint is the need to keep the antenna small to hide it from sight.

Since the antenna beam angle can be decreased by the use of a smaller wavelength as well as by a larger antenna, millimeter or even higher frequencies are sometimes viable alternatives to radio frequencies. The decision to use smaller wavelengths is tempered by such things as cost, available power, and propagation properties. The shorter wavelengths in general are attenuated more than the longer wavelengths and are more easily blocked by obstructions in their path. Furthermore, if the beam width is exceedingly narrow, it is difficult to keep it centered on another station of a communication network.

Time hopping, in which transmissions are increased in total duration, but contain pseudorandom time gaps, is another general countermeasure. Because of the pseudorandom gaps, an interception receiver

must either process more noise energy than it would otherwise or decrease its observation interval. In either case, performance degrades.

Spread-spectrum communications are inherently more difficult to intercept than are conventional communications. Frequency hopping over a wide bandwidth, a powerful countermeasure, complicates the design of an interception receiver and degrades its performance. Detection, frequency-estimation, and direction-finding difficulties increase with the hopping rate.

LITERATURE CITED

(1) A. Whalen, Detection of Signals in Noise, Academic Press, Inc., New York (1971).

(2) H. L. Van Trees, Detection, Estimation, and Modulation Theory, III, John Wiley and Sons, Inc., New York (1971).

(3) H. Urkowitz, Energy Detection of Unknown Deterministic Signals, Proc. IEEE, 55 (April 1967), 523.

(4) R. E. Ziemer and W. H. Tranter, Systems, Modulation and Noise, Houghton Mifflin Co., New York (1976).

(5) A. Papoulis, Signal Analysis, McGraw-Hill Book Co., New York (1977).

(6) R. A. Sprague, A Review of Acousto-optic Signal Correlators, Optical Engineering, 16 (September 1977), 467.

(7) D. L. Hecht, Spectrum Analysis Using Acousto-optic Filters, Optical Engineering, 16 (September 1977), 461.

(8) R. A. Coppock, R. F. Croce, W. L. Regier, Bragg Cell RF Signal Processing, Microwave J. (September 1978), 62.

(9) M. Engelson and F. Telewski, Spectrum Analyzer Theory and Applications, Artech House, Inc., Dedham, MA (1974).

(10) A. A. Oliner, ed., Acoustic Surface Waves, Springer-Verlag New York, Inc., New York (1978).

(11) H. J. Blinchikoff and A. I. Zverev, Filtering in the Time and Frequency Domains, John Wiley and Sons, Inc., New York (1976).

(12) D. K. Barton, Radar System Analysis, Artech House, Inc., Dedham, MA (1976).

(13) B. N. Mityashev, The Determination of the Time Position of Pulses in the Presence of Noise, McDonald, London (1965).

(14) D. J. Torrieri, Adaptive Thresholding Systems, IEEE Trans. Aerosp. Electron. Syst., 13 (May 1977), 273.

GLOSSARY OF PRINCIPAL SYMBOLS

a	Parameter proportional to bandwidth
A	Signal amplitude
$A(t)$	Amplitude modulation
b	Measure of beam width
B	Bandwidth of filter
d	Distance between two antennas
E	Signal energy
E_R	Root-mean-square error of direction estimate
$E[x]$	Expected value of x
f_c	Center frequency of filter (hertz)
f_s	Frequency of swept local oscillator (hertz)
f_0	Carrier frequency of intercepted signal (hertz)
$F(\theta)$	Beam pattern
$h(t)$	Impulse response of filter
$H(\omega)$	Filter transfer function
$I_n(x)$	Modified Bessel function of order n
L	Receiver output
$m(t)$	Binary message sequence
M	Number of channels in channelized radiometer
$n(t)$	White Gaussian noise
N	Number of comparator outputs examined during observation interval
N_0	Twice noise power spectral density
N_1	Number of comparator outputs examined during signal duration
$p(x)$	Probability density function
P_D	Probability of detection

64- Blank

GLOSSARY OF PRINCIPAL SYMBOLS (Cont'd)

P'_D	Probability that particular radiometer exceeds threshold when signal is present in that radiometer
P''_D	Probability that some radiometer exceeds threshold at end of sampling interval when signal is present
P_F	Probability of false alarm
P'_F	Probability that particular radiometer output exceeds threshold when no signal is present
r(t)	Received waveform, usually after bandpass filtering
R_s	Received power of intercepted signal
s(t)	Signal component
s'(t)	Waveform resulting from truncation of s(t)
$S(\omega)$	Fourier transform of s'(t)
T	Observation interval; period of single scan
T_d	Duration of impulse response of dispersive filter
T_r	Delay in arrival time of intercepted signal at one antenna output relative to arrival time at another output
T_s	Duration of sampling interval of channelized radiometer
T_1	Signal duration
v_a	Acoustic velocity
v_e	Electromagnetic velocity
V	Test statistic
V_T	Fixed threshold level of comparator
VAR(x)	Variance of x
W	Total bandwidth of system (hertz)
W_s	Bandwidth of constituent radiometers of channelized radiometer
α	Normalized peak value of response of scanning superheterodyne receiver
β	Parameter defined by equation (4)
β_1	Parameter defined by equation (44)

GLOSSARY OF PRINCIPAL SYMBOLS (Cont'd)

Υ	Largest integer less than or equal to TW
δ	Time delay due to filter or device
Δ	Resolution of frequency estimation system
ε	Parameter defined by equation (136)
η	Largest integer less than or equal to $T_s W_s$
θ	Phase angle; geometrical angle
λ	Noncentral parameter of chi-square distribution
Λ_a	Acoustic wavelength
Λ_o	Optical wavelength
Λ_s	Signal wavelength
μ	Rate of frequency change (hertz per second)
ξ	Parameter defined by equation (5)
ξ_1	Parameter defined by equation (45)
σ^2	Variance
ϕ	Arrival angle of intercepted signal
$\phi(t)$	Angle modulation function
χ^2	Chi squared, pertaining to probability distribution
ψ	Parameter related to maximum of radiation pattern
ω_c	Center frequency of filter (radians per second)
ω_s	Frequency of swept local oscillator (radians per second)
ω_0	Carrier frequency of intercepted signal (radians per second

DISTRIBUTION

ADMINISTRATOR
DEFENSE DOCUMENTATION CENTER
ATTN DDC-TCA (12 COPIES)
CAMERON STATION, BUILDING 5
ALEXANDRIA, VA 22314

COMMANDER
US ARMY MISSILE & MUNITIONS
CENTER AND SCHOOL
ATTN ATSK-CTD-F
REDSTONE ARSENAL, AL 35809

DIRECTOR
US ARMY MATERIEL SYSTEMS ANALYSIS
ACTIVITY
ATTN DRXSY-MP
ATTN DRXSY-CT
ABERDEEN PROVING GROUND, MD 21005

DIRECTOR
DEFENSE ADVANCED RESEARCH PROJECTS
AGENCY
ATTN DIR, TACTICAL TECHNOLOGY OFFICE
ARCHITECT BUILDING
1400 WILSON BLVD
ARLINGTON, VA 22209

DIRECTOR
DEFENSE COMMUNICATIONS ENGINEERING
CENTER
ATTN R&D OFFICE, ASST DIR FOR TECH
1860 WIEHLE AVE
RESTON, VA 22090

DIRECTOR OF DEFENSE
RESEARCH & ENGINEERING
ATTN DEP DIR (TACTICAL WARFARE PROGRAM)
WASHINGTON, DC 20301

ASSISTANT SECRETARY OF THE ARMY
(RES, DEV, & ACQ)
ATTN DEP FOR COMM & TARGET ACQ
ATTN DEP FOR AIR & MISSILE DEFENSE
WASHINGTON, DC 20310

COMMANDER
US ARMY COMMUNICATIONS-ELEC. COMMAND
ATTN STEEP-MT-M
FORT HUACHUCA, AZ 85613

OFFICE, DEPUTY CHIEF OF STAFF FOR
OPERATIONS & PLANS
DEPARTMENT OF THE ARMY
ATTN DAMO-TCD, ELECTRONIC/WARFARE
SIGNAL SECURITY
ATTN DAMO-RQZ
WASHINGTON, DC 20310

COMMANDER
US ARMY CONCEPTS ANALYSIS AGENCY
8120 WOODMONT AVENUE
ATTN MDCA-SMS
BETHESDA, MD 20014

COMMANDER
US ARMY COMMUNICATIONS R&D COMMAND
ATTN DRSEL-CE, COMMUNICATIONS-ELECTRONIC
SYS INTEG OFFICE
FORT MONMOUTH, NJ 07703

DIRECTOR, ELECTRONIC WARFARE LABORATORY
ATTN DELEW-V
ATTN DELEW-C
ATTN DELEW-E
ATTN DELEW-M-ST
FORT MONMOUTH, NJ 07703

COMMANDER
ELECTRONICS WARFARE LABORATORY
OFFICE OF MISSILE ELECTRONIC WARFARE
WHITE SANDS MISSILE RANGE, NM 88002

COMMANDER
NAVAL WEAPONS CENTER
ATTN CODE 35, ELECTRONIC WARFARE DEPT
CHINA LAKE, CA 93555

DIRECTOR
NAVAL RESEARCH LABORATORY
ATTN CODE 5700, TACTICAL ELEC
WARFARE DIVISION
WASHINGTON, DC 20375

COMMANDER
NAVAL SURFACE WEAPONS CENTER
ATTN DF-20, ELECTRONICS WARFARE DIV
ATTN DK, WARFARE ANALYSIS DEPT
DAHLGREN, VA 22448

DIRECTOR
AF AVIONICS LABORATORY
ATTN KL (WR), ELECTRONIC WARFARE DIV
WRIGHT-PATTERSON AFB, OH 45433

COMMANDER
HQ, TACTICAL AIR COMMAND
ATTN DOR, DIR OF ELECTRONIC
WARFARE OPNS
LANGLEY AFB, VA 23665

COMMANDER
HQ USAF TACTICAL AIR WARFARE
CENTER (TAC)
ATTN ER, DCS/ELECTRONIC WARFARE
AND RECONNAISSANCE
ATTN ERW, DIR OF ELECTRONIC
WARFARE
EGLIN AFB, FL 32542

68- Blank

US ARMY ELECTRONICS RESEARCH &
DEVELOPMENT COMMAND
ATTN TECHNICAL DIRECTOR, DRDEL-CT
ATTN DRDEL-CCM (3 COPIES)
ATTN DRDEL-ST
ATTN DRDEL-OP
ATTN TORRIERI, D., DRDEL-CCM (20 COPIES)
ADELPHI, MD 20783

INSTITUTE FOR DEFENSE ANALYSIS
400 ARMY NAVY DRIVE
ARLINGTON, VA 22209

DIA
DEP DIR OF SCIENTIFIC AND TECH INST
ELECTRONICS WARFARE BRANCH
1735 N. LYNN STREET
ARLINGTON, VA 22209

DEPT OF NAVY
OFFICE OF RES, DEV, TEST & EVAL
ATTN TACTICAL AIR SURFACE & EW DEV DIV
(NOP-982E5)
ATTN C&C EW AND SENSORS SEC
(NOP-982F3)
THE PENTAGON
WASHINGTON, DC 20350

COMMANDER
US ARMY TRAINING & DOCTRINE COMMAND
ATTN ATDC (DCS, COMBAT DEVELOPMENTS)
FT MONROE, VA 23651

OFFICE OF THE DEPUTY CHIEF OF STAFF
FOR RES, DEV, & ACQ
DEPARTMENT OF THE ARMY
ATTN DAMA-WS
ATTN DAMA-CS
ATTN DAMA-AR
ATTN DAMA-SCS, ELECTRONIC WARFARE TEAM
WASHINGTON, DC 20310

US ARMY COMBINED ARMS COMBAT DEV ACTIVITY
ATTN ATZLCA-CA
ATTN ATZLCA-CO
ATTN ATZLCA-FS
ATTN ATZLCA-SW
ATTN ATZLCA-COM-G
FT LEAVENWORTH, KS 66027

DIRECTOR
ELECTRONICS TECHNOLOGY & DEV LAB
ATTN DELET
FT MONMOUTH, NJ 07703

COMMANDER
US ARMY MATERIEL DEV & READINESS COMMAND
ATTN DRCPP
ATTN DRCPS
ATTN DRCDE
ATTN DRCDE-D
ATTN DRCBSI
5001 EISENHOWER AVENUE
ALEXANDRIA, VA 22333

DIRECTOR
US ARMY NIGHT VISION AND ELECTRO-OPTICS
LABORATORY
FT BELVOIR, VA 22060

COMMANDER
US ARMY COMBAT SURVEILLANCE AND
TARGET ACQUISITION LAB
FT MONMOUTH, NJ 07703

DIRECTOR
US ARMY SIGNALS WARFARE LAB
VINT HILL FARMS STATION
WARRENTON, VA 22186

COMMANDER
US ARMY INTELLIGENCE AND SECURITY COMMAND
ARLINGTON HALL STATION
ATTN IARDA (DCS, RDA)
ATTN IAITA (DIR, THREAT ANALYSIS)
4000 ARLINGTON BLVD
ARLINGTON, VA 22212

US ARMY TRADOC SYSTEMS ANALYSIS
ACTIVITY
ATTN ATAA-TDB
WHITE SANDS MISSILE RANGE, NM 88002

DIRECTOR
NATIONAL SECURITY AGENCY
ATTN S65
FT MEADE, MD 20755

HARRY DIAMOND LABORATORIES
ATTN 00100, COMMANDER/TECH DIR/TSO
ATTN CHIEF, 00210
ATTN CHIEF, 10000
ATTN CHIEF, 20000
ATTN CHIEF, 30000
ATTN CHIEF, 40000
ATTN RECORD COPY, 81200
ATTN HDL LIBRARY, 81100 (3 COPIES)
ATTN HDL LIBRARY, 81100 (WRF)
ATTN TECHNICAL REPORTS BR, 81300